2006

River, tidal and wind interactions in a deltaic estuarine system

Gregg Snedden
Louisiana State University and Agricultural and Mechanical College

RIVER, TIDAL, AND WIND INTERACTIONS IN A DELTAIC ESTUARINE SYSTEM

A Dissertation

Submitted to the Graduate Faculty of the
Louisiana State University and
Agricultural and Mechanical College
in partial fulfillment of the
requirements for the degree of
Doctor of Philosophy

in

The Department of Oceanography and Coastal Sciences

by
Gregg Snedden
B.S., University of Illinois at Urbana-Champaign, 1993
M.S., Louisiana State University, 1997
May 2006

ACKNOWLEDGEMENTS

I thank my major professor, Jaye Cable, for her guidance, flexibility and support over the last five years. Bill Wiseman showed limitless patience teaching the marvels of ocean physics to a biologist, and working with him has truly been a rich experience. I also want to thank committee members Andy Nyman, Chris Swarzenski, and Nan Walker for providing helpful comments that undoubtedly improved the quality of this dissertation.

My experience in coastal Louisiana has been amazing and would not have been possible without funding from the Environmental Protection Agency, the Natural Resources Conservation Service, and the Louisiana Department of Natural Resources. The U.S. Geological Survey and the Louisiana Department of Natural Resources provided much of the data used in this study. Delacroix Corporation's generosity was boundless. Their logistical support, including but not limited to five-star accommodations on the banks of Reggio Canal and occasionally getting us out of binds in the field (e.g., running out of gas, sunken airboats, etc.), is greatly appreciated. I thank Kate Wheelock for her help, dedication, and patience in the field. She is a great friend and I could not have asked for a better field partner. I also thank Emily Hyfield, Erick Swenson, Henri Delauney, Bryan Piazza, Guerry Holm, Dan Bond and Justin Baker for their field assistance. Thanks to all of my friends throughout my years in Louisiana. It has been an unforgettable experience. I especially thank Bryan, Sarai, and Sweetgrass for ensuring that I emerged from the frequency domain on the weekends. And Hilary, thanks for being there down the stretch and believing in me. Finally, I would like to thank my

parents, Al and Camille Snedden, and my sister, Suzette. You instilled in me a desire to always learn. I never could have pulled this off without your love and support.

TABLE OF CONTENTS

LIST OF TABLES

LIST OF FIGURES

ABSTRACT

The balance between river and marine influences is important in governing landscape sustainability in river deltas. River- and atmospherically driven sea level variability, sediment loading, and estuary-ocean exchange in the Mississippi River delta are examined in this study. Subtidal estuarine sea level variability in the Breton Sound estuary was driven by a combination of remote atmospheric forcing outside the estuary over the continental shelf and controlled river inputs through a gated diversion structure at the estuary head. The highly-frictional deltaic landscape acted as a low-pass filter to coastal fluctuations near the estuary mouth. When substantial quantities river water were discharged into the estuary, upper estuary sea levels responded to a combination of river and atmospheric forcing, while sea levels in the lower estuary responded only to coastal forcing. Annual sediment loading into Breton Sound through a Mississippi River diversion was approximately 1×10^5 metric tons yr^{-1}. Four pulsed, high-discharge diversions were conducted during the study, and sediment loading across each pulse was highly variable and was greatest during rising limbs of Mississippi River floods. Overland flow was induced when diversion discharge exceeded 100 $m^3 s^{-1}$. These results indicate timing and magnitude of diversion events are both important factors governing marsh sediment deposition in river diversion receiving basins. Sediment inputs measured during this study were negligible compared to historical loading through crevasses in the region. An investigation of estuary-shelf exchanges through Barataria Pass revealed that tidal exchange accounted for approximately 80% of the observed flow variability. Two dominant vertical subtidal exchange modes were identified. A barotropic mode, which accounted for most of the flow variance, was most coherent with cross-shelf wind stress.

A second mode resembling baroclinic estuarine circulation recurred over fortnightly timescales, apparently in response to variations in tidal stirring. The baroclinic mode also appeared to be modulated by variability in freshwater inputs to the estuary. These findings provide a greater understanding of the physical dynamics that govern landscape sustainability in microtidal river deltas.

CHAPTER I.

INTRODUCTION

Considerable effort has been put forth toward understanding circulation patterns in estuaries and linking these patterns to specific forcing mechanisms. Knowledge of these linkages is important, as estuarine circulation patterns can influence characteristics that are important to ecosystem structure and function. Estuarine circulation governs inundation and salinity regimes, which in turn dictate soil chemistry and nutrient inputs to surrounding wetlands, and ultimately determine biotic parameters such as species composition and productivity rates (Mitsch and Gosselink 1993). Circulation also controls phenomena such as recruitment of larval fauna from the continental shelf (Shaw et al. 1985; Epifanio 1995; Brown et al. 2000).

Pritchard (1955) provided the first dynamic description of estuarine circulation, in which gravity acts on horizontal differences in density to create a flow pattern with denser sea water flowing landward under less dense seaward-flowing fresh water. Limited mixing between the layers alters the horizontal density gradient, which subsequently affects the gravitational circulation. Their descriptions came from observations on the James River, a partially mixed estuary, where average river discharge into the estuary is small relative to tidal flow in and out of the estuary.

Data used to derive Pritchard's gravitational circulation model were obtained with non-recording equipment that required continuous attendance by field personnel, and as a result data collection for these efforts was conducted in relatively calm weather and generally did not exceed ten days. Thus, the gravitational circulation model of estuarine circulation represents a kind of steady-state where meteorological variables and river

discharge are relatively constant. While Pritchard's model has been quite useful in serving as a foundation for our understanding of estuarine circulation, energy inputs from storm events and fluctuations in river discharge are not taken into account, making the model overly simplistic for longer timescales that may encompass synoptic weather events. These processes are particularly important in well mixed estuaries where gravitational circulation is weak. They are also the primary transport mechanism in microtidal estuaries where atmospherically-induced fluctuations can exceed astronomically-induced motions by an order of magnitude.

In the mid 1970s, with the advent of continuously-recording instruments, it became possible to obtain much longer data records that would capture these low-frequency oscillations. Weisberg and Sturges (1976) showed that intermediate to the non-fluctuating, density-driven gravity circulation and semi-diurnal tidal flushing was a wide range of temporal scales over which velocities fluctuated in Narragansett Bay. Further analysis showed 97% of the current velocity variance could be explained by the wind across the most energetic part of the current velocity spectrum (Weisberg 1976).

Elliott (1978) identified two dominant spatial patterns of atmospherically-induced low-frequency current and water-level variability in the Potomac River estuary. One pattern accounted for 53% of the total variability and described a sea-surface slope response, while the second pattern described a barotropic response in which water levels at the upper and lower ends of the estuary responded equally and in-phase with each other. This second mode of variability accounted for 26% of the variability. A follow-up to this study (Elliott and Wang 1978) attributed the slope response to local forcing caused by wind blowing directly along the axis of the estuary, while the longer-period barotropic

response was associated with estuary-shelf exchanges remotely forced by alongshore wind stress and subsequent Ekman set up and set down of shelf waters. Wang and Elliott (1978) more closely examined non-local forcing mechanisms. The authors determined that Chesapeake Bay water was actually driven out of the estuary during an up-estuary wind. While clearly inconsistent with local wind forcing, these observations were very much in agreement with remote along-shore winds causing Ekman set down and subsequent release of estuarine waters onto the adjacent shelf.

Much coastal physical oceanographic research over the last 25 years has focused on the effects of local and non-local forcing. Variability in subtidal estuarine water levels and currents being driven by one or both of these mechanisms has been observed in drowned-river valleys where estuary-shelf exchange is relatively uninhibited (e.g. Delaware Bay; Wong and Garvine 1984; Janzen and Wong 2002), as well as systems where exchange processes are frictionally constrained by sills (e.g. Puget Sound, WA; Mofjeld 1992) or tidal passes (e.g. Corpus Christi Bay, TX; Smith 1977; Calcasieu Lake, LA; Lee et al. 1990). Garvine (1985) used an analytical model to verify the influence of these two processes on estuarine sea levels. The model shows that the relative importance of the remote effect decreases with increasing estuary length and that the orientation of the length axis of the estuary relative to that of the regional coastline is important in determining how the remote and local effects interact with each other. Distinguishing between locally- and remotely- induced motions is important because they have fundamentally different effects on the estuary. While remotely-forced motions cause exchanges of water and materials between estuaries and their adjacent shelves,

locally-forced motions simply result in a redistribution of existing water within the estuary.

While estuarine response to local and remote wind forcing is now well-documented, relatively few studies have addressed the influence of riverine inputs on time-varying subtidal currents and water levels in these systems. This knowledge gap may partially result from the difficulty of resolving the longer-period oscillations typical of river runoff patterns with data spanning a rather limited time interval. In the Delaware estuary, coherence of sea level with wind stress at low frequencies decreased with increasing distance from the mouth of the estuary, suggesting that some other factor, perhaps runoff from the Delaware River, was governing variability at these timescales in the upper reaches (Wong and Moses-Hall 1998). In Weeks Bay, AL, consistencies were found between river discharge events and both water level and exchange of water with Mobile Bay (Schroeder et al 1990), but because of the relatively short length of the data record, not enough runoff events were captured to establish a statistical relationship between the signals. Wu (1991) documented that water level at all stations in the Pearl River delta, China, were coherent with river discharge, with the amplitude of the transfer function relating discharge to water levels decreasing toward the seaward end of the estuary. These observations imply that Pearl River discharge induces a slope effect on water levels in the estuary. River-induced sea-surface slope induction has also been documented in Mobile Bay (Schroeder and Wiseman 1986).

Most of the world's coastal wetlands are located in deltas (Day et al. 1997) and they are economically and ecologically important. Deltas are generally highly populated regions, and as such are affected by a variety of anthropogenic impacts such as

impoundment, isolation from fluvial inputs, water and minerals extraction, and the construction of oilfield canals. These circumstances have resulted in a myriad of problems, including increased subsidence rates, reduced accretion rates, salinity intrusion, and reduced biological productivity. One effect of these impacts is relative sea level rise (RSLR), an apparent increase in local sea level due to a combination of eustatic sea level rise and subsidence. RSLR is occurring at alarming rates in virtually all of the world's major river deltas, with rates ranging from 1-3 mm yr^{-1} in the Po delta, Italy (Carbognin et al. 2004), up to 12 mm yr^{-1} in the Yangtze delta, China (Xiqing 1998).

The relative influence of fluvial and marine forcing plays an important role in governing the sustainability of deltaic landscapes. A critical difference between land building and land loss in wetlands is the rate at which sedimentation and organic matter accumulation occur relative to rates of RSLR. Marsh inundation events can result in either case, depending on the source of the floodwaters. Flooding associated with river inputs can deliver mineral sediments to the subsiding marsh, facilitating sedimentation (Wheelock 2003) and enhancing organic matter accumulation (Nyman et al. 1990). Though flooding associated with inflows of continental shelf waters into the estuary brought about by wind-forced setup at the coast can also deliver sediments to wetland communities in the delta (Roberts 1997), it is also a principal mechanism for saltwater intrusion. The intrusion of saline waters can stress fresh marsh communities (McKee and Mendelssohn 1989) and decrease root formation that can account for much of the vertical accretion in a healthy marsh (Nyman et al. 1990). This decreased accretion can accelerate RSLR and ultimately coastal land loss.

Rates of RSLR approaching 10 mm yr^{-1} have been observed in some regions of the Mississippi River delta in southeast Louisiana (Coleman et al. 1998), and have contributed to a situation where, statewide, annual coastal land loss rates have approached 115 km^2 yr^{-1} (Barras et al. 1994). Though an entire suite of factors have contributed to this, isolation of the Mississippi River by containment levees is generally regarded as a primary factor. In an effort to mitigate this problem, multiple controlled river diversions have either been implemented or are in the planning stages. It is widely perceived that these measures will help reduce saltwater intrusion, subsidize coastal wetland communities with nutrients, and provide a source of mineral sediments to the subsiding deltaic landscape.

My dissertation examines the interactions of wind, river, and tidal influences on water levels, sediment loading, and estuary-shelf exchange in two subestuaries of the Mississippi River delta. In chapter two, I examine the relative influences of remote and local atmospheric forcing and river inputs through the Caernarvon Freshwater Diversion Structure on subtidal water variability in the Breton Sound estuary. Empirical frequency-dependent relationships between forcing functions and sea level responses at two locations in the estuary are estimated. A frequency-dependent analytical model is used to compare the sea level response of the highly frictional Breton Sound estuary to deeper, less frictional systems where atmospherically-induced sea level variability has been previously studied. In chapter, three I examine the impact of a pulsed river diversion management plan on sediment loading into the Breton Sound estuary. Variability in sediment delivery among four controlled releases of river water into the estuary are related to hydraulic conditions on the Mississippi River. A mass balance approach is

used to examine trends in overland flow in the receiving basin and how they relate to diversion discharge. Finally, sediment delivery associated with the pulsed diversions is compared with delivery associated with historical diversions along the Mississippi River. In chapter four, estuary-ocean exchanges through Barataria Pass are examined to assess the importance of wind, river, and tidal influences on variability of flow through the pass. Tidal excursions are estimated, and subtidal flows are decomposed into two vertical modes of variability. Relationships between these modes of flow variability and wind, river, and tidal forcing are then explored. A brief summary is given in chapter five.

Literature Cited

Barras, J.A., P.E. Bourgeois, and L.R. Handley. 1994. Land loss in coastal Louisiana 1956-90. National Biological Survey, National Wetlands Research Center Open File Report 94-01 4 pp. 10 color plates.

Brown, C.A., G.A. Jackson, and D.A. Brooks, 2000. Particle transport through a narrow tidal inlet due to tidal forcing and implications for larval transport. Journal of Geophysical Research 105: 24141-24156.

Carbognin, L.,P. Teatini, and L. Tosi. 2004. Eustacy and land subsidence in the Venice Lagoon at the beginning of the new millennium. Journal of Marine Systems 51: 345-353.

Coleman, J.M., H.H. Roberts, and G.W. Stone. 1998. Mississippi River delta: An overview. Journal of Coastal Research 14: 698-716.

Day, J.W., Jr., J.F. Martin, L. Cardoch, and P.H. Templet. 1997. System functioning as a basis for sustainable management of deltaic ecosystems. Coastal Management 25: 115-153.

Elliott, A.J.. 1978. Observations of the meteorologically induced circulation in the Potomac Estuary. Estuarine and Coastal Marine Science 6: 285-299.

Elliott, A.J. and D.P. Wang. 1978. The effect of meteorological forcing on the Chesapeake Bay: the coupling between and estuarine system and its adjacent coastal waters. In: Hydrodynamics of Estuaries and Fjords (ed. J.C.J. Nihoul), Elsvier Scientific Pulb. Co., Amsterdam, pp 127-145.

Epifanio, C. 1995. Transport of blue crab (*Callinectes sapidus*) larvae in the waters off the Mid-Atlantic states. Bulletin of Marine Science 57: 713-725.

Garvine, R.W.. 1985. A simple model of estuarine subtidal fluctuations forced by local and remote wind stress. Journal of Geophysical Research 90: 11945-11948.

Janzen, C.D. and K.C. Wong. 2002. Wind-forced dynamics at the estuary-shelf interface of a large coastal plain estuary. Journal of Geophysical Research 107 (C10), 3138, doi:10.1029/2001JC000959.

Lee, J.M., W.J. Wiseman, Jr., and F.J. Kelly. 1990. Barotropic, subtidal exchange between Calcasieu Lake and the Gulf of Mexico. Estuaries 18: 258-264.

McKee, K.L., and I.A. Mendelssohn. 1989. Response of a freshwater marsh plant community to increased salinity and increased water level. Aquatic Botany 34: 301-316.

Mitsch, W.J. and J.G. Gosselink. 1993. Wetlands. 2nd Edition. 722 pp. Van Nostrand Reinhold, New York.

Mofjeld, H.O. 1992. Subtidal sea level fluctuations in a large fjord system. Journal of Geophysical Research 97: 20191-20199.

Nyman, J.A., R.D. DeLaune, and W.H. Patrick, Jr. 1990. Wetland soil formation in the rapidly subsiding Mississippi River deltaic plain: mineral and organic matter relationships. Estuarine, Coastal and Shelf Science 31: 37-52.

Pritchard, D.W. 1955. Estuarine circulation patterns. Proceedings of the American Society of Civil Engineers 81: No. 717.

Roberts, H.H. 1997. Dynamic changes of the Holocene Mississippi River Delta plain: the delta cycle. Journal of Coastal Research 13: 605-627.

Schroeder, W.W. and W.J. Wiseman, Jr. 1986. Low-frequency shelf-estuary exchange processes in Mobile Bay and other estuarine systems in the northern Gulf of Mexico. In: Estuarine Variability (Ed. D.A. Wolfe), Academic Press, Orlando, FL, pp. 355-367.

Schroeder, W.W., W.J. Wiseman, Jr., and S.P. Dinnel. 1990. Wind and river induced fluctuations in a small, shallow, tributary estuary. In: Residual Currents and Long Term Transport (ed. R.T. Cheng). Springer-Verlag, New York, pp. 481-493.

Shaw, R.F., W.J. Wiseman, R.E. Turner, L.J. Rouse, R.E. Condrey, and F.J. Kelly. 1985. Transport of larval Gulf menhaden *Brevoortia patronus* in continental shelf waters of western Louisiana: a hypothesis. Transactions of the American Fisheries Society 114: 452-460.

Smith, N. P. 1977. Meteorological and tidal exchanges between Corpus Christi Bay, Texas, and the northwestern Gulf of Mexico. Estuarine, Coastal and Shelf Science 5: 511-520.

Wang, D.P. and A.J. Elliott. 1978. Non-tidal variability in the Chesapeake Bay and Potomac River: evidence for non-local forcing. Journal of Physical Oceanography 8: 225-232.

Weisberg, R.H. 1976. The nontidal flow in the Providence River of Narragansett Bay: a stochastic approach to estuarine circulation. Journal of Physical Oceanography 6: 721-934.

Weisberg, R.H. and W. Sturges. 1976. Velocity observations in the west passage of Narragansett Bay: a partially mixed estuary. Journal of Physical Oceanography 6: 345-354.

Wheelock, K.W. 2003. Pulsed river flooding effects on sediment deposition in Breton Sound Estuary, Louisiana. M.S. Thesis. Louisiana State Univ., Baton Rouge, Louisiana, USA.

Wong, K.C. and R.W. Garvine. 1984. Observations of wind-induced, subtidal variability in the Delaware Estuary. Journal of Geophysical Research 89: 10589-10597.

Wong, K.C. and J.E. Moses-Hall. On the relative importance of the remote and local wind effects to the subtidal variability in a coastal plain estuary. Journal of Geophysical Research 89: 18393-18404.

Wu, C. 1991. Response of the Pearl River estuarine complex to the meteorological forcing and river inflow: a cybernetics approach. Journal of Coastal Research 7: 1153-1167.

Xiqing, C. 1998. Changjian (Yangtze) River Delta, China. Journal of Coastal Research 14: 838-858.

CHAPTER II.

SEA LEVEL VARIABILITY IN A MISSISSIPPI RIVER DELTAIC ESTUARY, LOUISIANA

Introduction

Considerable effort has been put forth in recent decades to understand wind and tide-induced motions in estuaries. Two decades after Pritchard (1955) put forth the steady-state gravitational estuarine circulation model, use of continuously-recording instruments enabled the collection of long term data sets which captured multiple passages of synoptic weather systems. Since then, the importance of estuarine motions over 3 to 20 day time scales has been clearly recognized (Weisberg 1976; Elliott and Wang 1978; Wang 1979). Often these meteorologically-induced exchanges can far exceed those driven by astronomical tides.

Several studies in relatively deep (>10 m) estuaries located primarily along the North American Atlantic coast have shown how atmospheric influences on estuarine water level variability can occur through two dynamic processes (Elliott and Wang 1978; Wang 1979; Wong 1990; Wong and Moses-Hall 1998; Janzen and Wong 2002). Local wind stress directly over the estuary surface can induce a sea level slope in which water levels are highest in the downwind portion of the system, and coastal winds at remote locations outside the estuary can induce cross-shelf Ekman transport which results in sea-level co-oscillations between the estuary and the adjacent continental shelf. These dynamics have been verified with analytical models (e.g. Garvine 1985), which have shown that the relative importance of the local effect becomes greater with increasing distance from the estuary mouth. In relatively deep estuaries with free communication to the continental shelf, frictional damping of remotely-forced sea level oscillations is

typically absent, and amplitudes of these fluctuations throughout the estuary are spatially-uniform.

Other investigations have illustrated the influence that river forcing exerts on estuarine subtidal circulation. Coherence of subtidal surface and bottom currents with river discharge has been documented in the western region of Long Island sound at frequencies below 0.15 cycles/day (cpd; Filadelfo et al. 1991), with depth-varying phase relationships consistent with a baroclinic response to buoyancy forcing. Similar subtidal baroclinic responses of estuarine currents to river inflows have been observed in coastal lagoons of Delaware (Janzen and Wong 1998) and in Mobile Bay, Alabama (Noble et al. 1996). Clear responses in the structure of the salinity field, across both horizontal (Garvine et al. 1992; Wong 1995) and vertical (Schroeder et al. 1990) dimensions, have been observed. However, relatively little attention has been given to the effects of river inflows on estuarine water levels, perhaps because in many systems the sea level response to discharge events is minimal when compared to responses forced by tidal and atmospheric phenomena. Nevertheless, potential impacts of river-forced sea level fluctuations are evident in some systems. In coastal Louisiana, near the delta of the Atchafalaya River, the fifth largest river in the world in terms of discharge (Iseri and Langbein 1974), coastal marshes are flooded nearly 40% of the time during high river discharge (Stern et al. 1991). In Weeks Bay, Alabama, qualitative consistencies were found between river discharge events and bay sea level (Schroeder et al. 1990), but due to the relatively short length of the data record, not enough runoff events were captured to establish a statistical relationship between the signals. And in Delaware Bay, multiple coherence of upper estuarine sea level with local and remote wind forcing diminishes

severely at very low frequencies (Wong and Moses-Hall 1998), suggesting that some other mechanism, likely river forcing, governs sea level over these time scales.

The subestuaries of the Mississippi River delta along the northern Gulf of Mexico (GOM) coast exhibit fundamental differences from their east coast counterparts. Semi-diurnal tides along the northern GOM coast are notably absent, and diurnal ranges during spring tides are on the order of 40 cm, indicating a relatively larger portion of the energy in the sea level spectrum exists in the subtidal frequency bands. These estuaries are generally quite shallow (<2.5 m), typically consisting of a matrix of periodically-flooded coastal marshes and ponds intermixed with a network of shallow lakes, oil-field canals and circuitous bayous. Presumably these features have the effect of reducing fetch and increasing hydraulic friction when compared to "typical" pelagic systems found along the Atlantic coast where atmospherically-forced estuarine motions have been more extensively examined. Unlike deep, pelagic estuaries where coastally-induced sea level variations are either minimally dampened by friction or in some cases even enhanced by resonance, frictional damping of these motions in the upper reaches of shallow, microtidal estuaries of the Mississippi River delta may render astronomically-induced fluctuations inconsequential, and significant damping can extend well into frequencies of the synoptic weather band. Thus, absent river-forced sea level variability, delivery of materials and biota to the marshes of these systems, and their subsequent export to the GOM, may be almost entirely governed by the passage of strong meteorological forcing events.

This study examines the influence of fluvial, atmospheric and tidal forcing on estuarine water-level variability in Breton Sound, a frictionally-dominated deltaic

estuary. Situated in southeastern Louisiana on the Mississippi River deltaic plain, the estuary receives controlled Mississippi River inputs through a gated diversion structure located at the estuary head. The remainder of this paper will 1) examine the relative importance of local and remote components of atmospheric forcing, 2) determine how river forcing may modulate atmospherically-induced sea-level variability, 3) characterize spatial and temporal trends in the relative importance of river and atmospheric forcing, 4) examine spatial patterns of tidal variability in the estuary, and 5) compare the relative importance of these forcings in this highly frictional system with those previously observed in deeper, open-water systems.

The Study Area and Data

Breton Sound is a bar-built estuary located on the eastern side of the Mississippi River immediately southeast of New Orleans, Louisiana (Figure 1). Its longitudinal axis is oriented about 120^{o} clockwise from true north, and it is approximately 40 km long. Breton Sound is a deltaic landscape containing marshes, barrier islands, lakes, abandoned Mississippi River distributary channels, and natural levees that are the product of over 4000 years of fluvial inputs and delta switching processes (Roberts 1997). Throughout most of the 20^{th} century these marshes have been isolated from direct riverine influxes by containment levees along the river and are now in the abandonment phase of the delta cycle where high rates of land loss occur largely due to reductions in sediment supply (Coleman et al. 1998).

Astronomical tides in the lower estuary are primarily diurnal and generate currents with typical spring tide velocities of 0.1 m s^{-1}. The K_1 and O_1 constituents dominate the tidal signal, and amplitudes of 14 cm near the estuary mouth indicate the

system is microtidal. Owing to the large tidal flux (on the order of 1000 $m^3 s^{-1}$) relative to average freshwater input (40 $m^3 s^{-1}$), its shallow depth (1.5 m), and the importance of wind-induced mixing in the system, Breton Sound can be classified as a weakly stratified estuary.

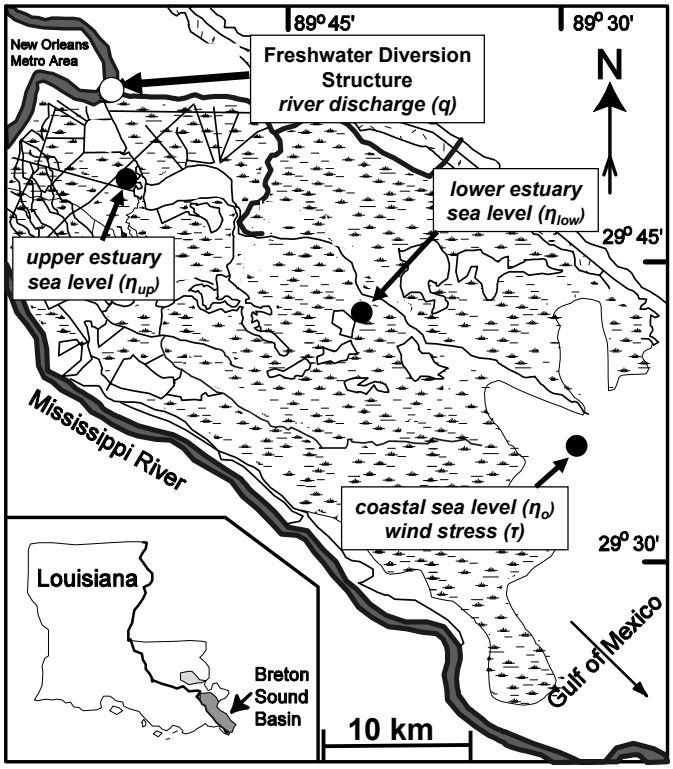

Figure 2.1. Map of study area showing stations where sea level, freshwater discharge, and wind stress data were collected.

Subtidal motions in the estuary are largely affected by Mississippi River inflows and sea-level oscillations in the shelf waters of the GOM. These oscillations over the continental shelf are driven by a combination of buoyancy forcing from the mouth of the Mississippi River as it enters the GOM, thermosteric fluctuations of GOM waters, and shelf-slope exchanges driven by alongshore wind stress and associated Ekman transports (Current 1996). A semi-annual cycle in GOM sea-level exists, which generally exhibits a

maximum during early autumn, a minimum during winter, a secondary maximum during spring and a secondary minimum during summer (Marmer 1954). Controlled river inflows to the Breton Sound estuary occur through a gated river diversion structure located at the head of the system, (80 km upstream from the Head of Passes on the Mississippi River; Figure 2.1). The structure has a discharge capacity of 225 $m^3 s^{-1}$ and delivers on the order of 1 X 10^8 kg of Mississippi River sediments to Breton Sound each year. The structure has been operational since 1991, and was designed to moderate salinities and re-introduce fluvial inputs to the estuary. River discharge through the structure generally follows an annual pattern, with the largest releases of river water occurring during spring.

Hourly sea-level data, collected by the U.S. Geological Survey Water Resources Division in Baton Rouge, were obtained with pressure transducers at a station in the upper estuary (η_{up}), the lower estuary (η_{lo}), and at a coastal station immediately outside the estuary (η_o; Figure 1) from January 1999 through October 2002. The transducers were vented to the atmosphere to provide sea level data that were not influenced by atmospheric pressure variations. Wind velocity was measured hourly at Bay Gardene (Figure 1) and used to estimate wind stress (τ) following Large and Pond (1981). Discharge of Mississippi River water entering the estuary through the diversion structure (q) was measured daily. Because all other variables were measured hourly, the daily values of diversion discharge were spline-interpolated to produce estimates of hourly discharge. Because the sea level data contain oscillations at both the tidal and subtidal frequencies, all time series were passed through a Lanczos filter (Bloomfield 1976) with a cutoff period of 33 h to separate the tidal variations from subtidal fluctuations.

Subtidal Variations

Remote and Local Atmospheric Forcing

Effects of atmospheric forcing were examined by analyzing time-series data collected from September to November in the years 1999 through 2001. These time periods were chosen because freshwater inputs through the diversion structure were minimal ($\overline{q} < 10$ m^3 s^{-1}). It was assumed that during these time periods subtidal sea level variability in the estuary was primarily driven by a combination of local and remote atmospheric forcing. A fast Fourier transform algorithm was used to estimate spectra and cross-spectra, which were smoothed with a 5-point boxcar filter. Spectra and cross-spectra from each 3-month period were then ensemble-averaged across the three years and used to estimate transfer functions and coherence and phase spectra. Thus, each individual spectral estimate in the ensemble-averaged spectra and cross-spectra was comprised of 15 data points, yielding 30 degrees of freedom. The 95% significance level for coherence estimates was 0.19. Confidence intervals (95%) for phase and transfer function moduli were estimated according to Jenkins and Watts (1998).

To investigate the effects of local wind stress forcing, I first examined the relationship between τ, defined as the wind stress component blowing upestuary (positive toward 300ºT), and sea surface slope. Measured sea-surface slope in this study is defined as

$$\frac{\Delta\eta}{\Delta x} = \frac{\eta_{up} - \eta_o}{x_{up} - x_o}, \qquad \textbf{(2.1)}$$

where x_{up} and x_o are straight-line distances from the estuary mouth to the upper estuary and coastal sea level stations, respectively. Thus, a positive value for sea surface slope indicates a situation where estuarine sea levels exceed those observed at the coastal

ocean. The root mean square of measured sea surface slope was 4.1×10^{-6}, with minimum and maximum values -1.8×10^{-5} and 1.1×10^{-5}, respectively.

Assuming the low-frequency sea surface slope is essentially in balance with the local wind stress forcing, the expected sea-surface slope response can be described by

$$\frac{\partial \eta}{\partial x} = \frac{\tau}{\rho g h}, \qquad \textbf{(2.2)}$$

where ρ is the mean density of estuarine water, g is the gravitational acceleration constant, and h is the average depth of the estuary. Equation (2.2) thus describes a situation in which wind stress blowing upestuary induces a positive slope where estuarine sea levels exceed those at the coastal ocean, and implies that τ and $\frac{\Delta \eta}{\Delta x}$ should vary in phase with each other. Cross-spectral analysis showed phase between measured sea surface slope and along-estuary wind stress is near 180º across timescales where coherence between the two signals is significant (Figure 2.2), indicating that dynamics other than a balance with local wind stress forcing must be responsible for sea surface slope induction within the estuary.

To determine the wind stress directional component most effective at forcing coastal sea level fluctuations, ordinary coherence spectra were computed between η_o and the north-south (0^o) wind stress component, and each subsequent wind stress component through 180^o at 10^o intervals (Figure 2.3a). Fluctuations in η_o were most coherent with wind stress along the $100^o/280^o$ component (positive toward 100^o); phase angle along this directional component was near 180^o across all frequencies (Figure 2.3b). Together, the coherence and phase spectra indicate that winds blowing eastward along the shelf cause

reductions in coastal sea levels, and suggest that coastal sea level fluctuations near the mouth of the Breton Sound estuary are largely governed by Ekman convergence at the coast.

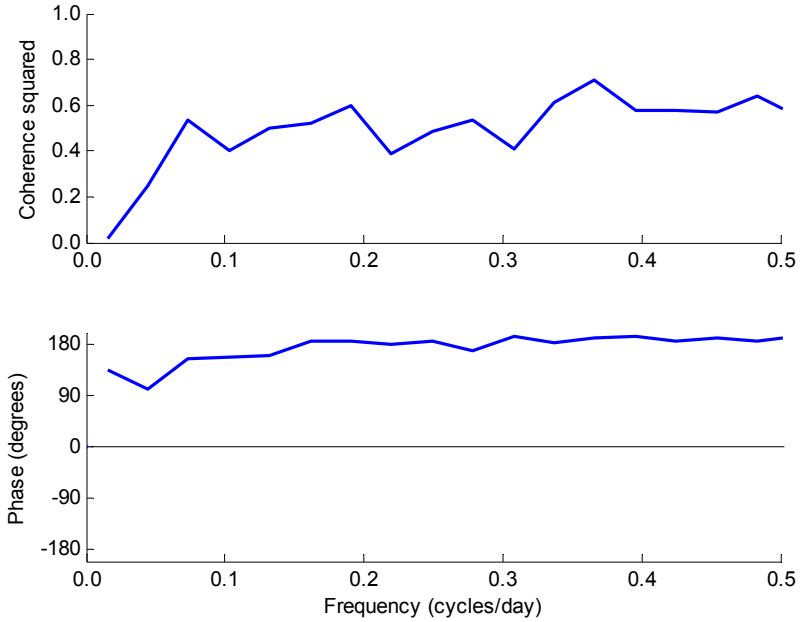

Figure 2.2. Coherence (upper) and phase (lower) between along estuary wind stress (positive toward 300ºT) and sea surface slope.

Because various forcing functions (i.e., local, along-estuary and remote, along-shelf winds) may be correlated with each other in addition to being correlated with the output variable, partial coherence and transfer functions were estimated for all further analyses (Bendat and Piersol 1993). Assuming freshwater input during the September-November time period is unimportant, sea level at a point in the estuary can be described by a spectral model

$$\hat{\eta}_x = a\hat{\eta}_o + b\hat{\tau} + \hat{\varepsilon} \qquad \textbf{(2.3)}$$

where the circumflex indicates the Fourier transform of the corresponding variable, η_x is sea level at distance x from the estuary mouth, ε is the noise or residual error, and the

coefficients a and b are complex transfer functions, relating η_o and τ, respectively, to estuarine sea level fluctuations. The proportion of the total variance explained by the two inputs as a function of frequency is indicated by the multiple coherence spectrum of the model.

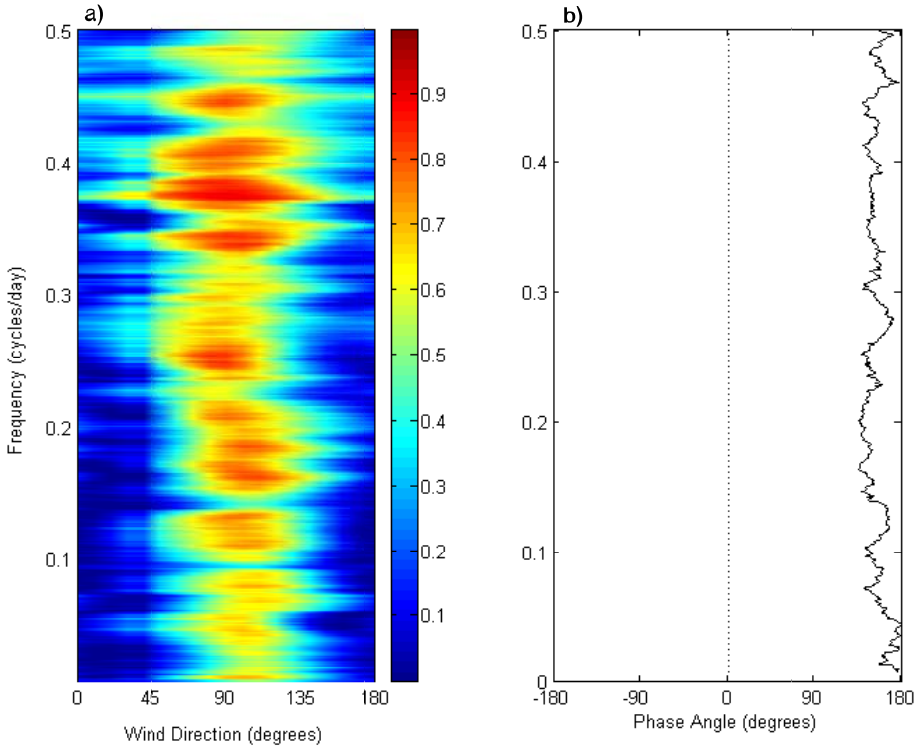

Figure 2.3. (left) Coherence squared between η_o and wind stress components along the directions of 0^o – 180^o in 10^o increments. (right) Phase relationship between alongshore wind stress (positive toward 100^o) and η_o.

Results of the partial coherence analysis indicate that the two inputs together can explain nearly all the sea level variability in the lower estuary (Figure 2.4a), and much of the variability in the upper estuary (Figure 2.4b), although multiple coherence in the upper basin diminishes with increasing frequency. At both locations, partial coherence of sea level with along-estuary wind stress is very low, suggesting that its role in governing sea-level variability in the estuary is negligible. Partial coherence of water level with η_o

is considerably higher, indicating that fluctuations at the marine boundary are important determinants of estuarine sea levels.

The linear systems model described by (2.3) can be used to construct coherent output power spectra, which estimate the relative contributions to the output (η_x) variability attributable to each forcing function (η_o, τ) for a given frequency. This procedure is accomplished by multiplying (3) by its complex conjugate to yield

$$\begin{aligned}\left\langle \hat{\eta}_x \hat{\eta}_x^* \right\rangle = \left\langle aa^* \right\rangle \left\langle \hat{\eta}_o \hat{\eta}_o^* \right\rangle + \left\langle bb^* \right\rangle \left\langle \hat{\tau}\hat{\tau}^* \right\rangle \\ +2\,\mathrm{Re}\left\langle ab^* \right\rangle \left\langle \hat{\eta}_o \hat{\tau}^* \right\rangle + \left\langle \hat{\varepsilon}\hat{\varepsilon} \right\rangle\end{aligned} \qquad \textbf{(2.4)}$$

where $\langle\ \rangle$ indicates spectral averaging and (*) denotes the complex conjugate. In (2.4), the first and second terms on the right hand side represents the contribution by the coastal sea level and along-estuary wind stress autospectra, respectively. The third term represents the contribution by the cross-spectrum of the forcing functions, and the last term is the residual variation, or noise. At both estuarine water level stations, the major contribution to the output variance is from coastal sea level fluctuations, while the variance of the autospectral term associated with along-estuary wind stress is near zero across all subtidal frequencies (Fig 2.4 c,d). Appreciable variability exists in the cross-spectral term at the upper estuary location, and it is not possible to assign the energy contained in this term to a particular forcing input. However, even if all of the energy contained in the cross-spectral term is arbitrarily assigned to local wind forcing, the variability attributable to the remote autospectral term still dominates the system. Thus, across subtidal time scales, it is clear that direct forcing by local wind stress in the Breton Sound estuary plays a minor role when compared to the effects of remote atmospheric forcing.

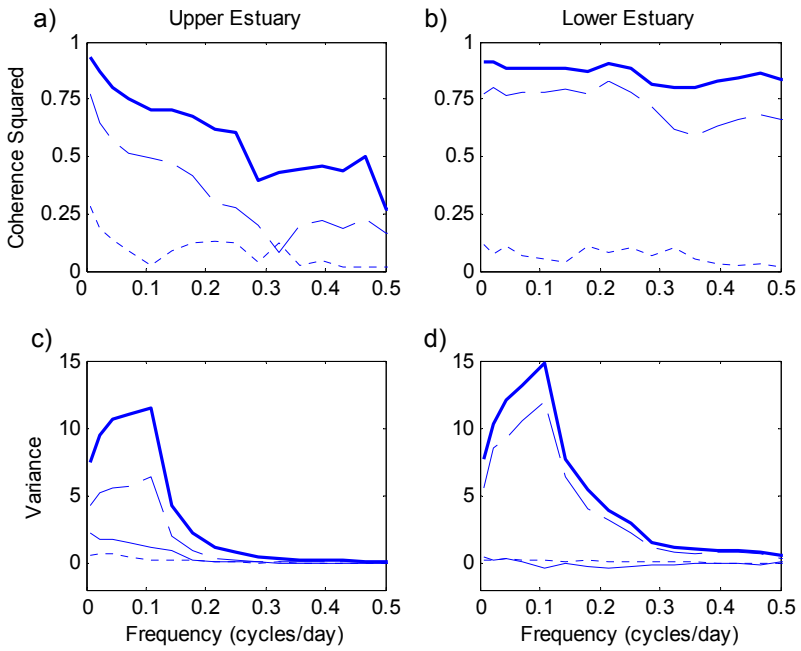

Figure 2.4. (top) Multiple coherence (thick, solid line) of η_o and τ with upper (a) and lower (b) estuary sea level. Partial coherence of η_o (long, dashed line) and τ (dotted line) with estuarine sea levels are also shown. (bottom) Observed upper (c) and lower (d) estuary sea level power spectra (thick, solid line). Also shown are variance contributions from η_o (long, dashed line) , τ (dotted line), and η_o and τ cross-spectrum (thin solid line).

To a large degree, the relative unimportance of local wind forcing in the Breton Sound estuary may be explained by the landscape features unique to deltaic systems. The estuary consists largely of numerous narrow, circuitous channels that are separated by marsh and natural or anthropogenic levees (Figure 2.1). Because of these features, local winds can never generate an appreciable slope response on the system due to limitations in fetch. Thus, to a first approximation, forcing by local wind stress may be considered negligible in the estuary. As a result, atmospheric forcing in this system acts almost entirely by inducing set up and set down of coastal waters through Ekman dynamics.

Riverine and Remote Atmospheric Forcing

The relative roles of riverine and remote atmospheric forcing on estuarine sea levels are now examined. The statistical model becomes

$$\hat{\eta}_x = a\hat{\eta}_o + c\hat{q} + \hat{\varepsilon} \quad \textbf{(2.5)}$$

where q is freshwater discharge through the diversion structure and c is a complex transfer function relating freshwater discharge to estuarine sea level. Factors involving local wind stress effects (b, τ) are excluded in this model because they were determined above to be unimportant in governing estuarine water levels. The model was used to compare variance partitioning between two time periods in the upper and lower estuary. One of these time periods, called "spring" for brevity, is the three month period from January through March, while the other, called "autumn" is the three month period from August through October. These two time periods were chosen because they differ by nearly an order of magnitude in terms of mean freshwater discharge through the diversion structure ($\overline{q}$ = 62 m^3 s^{-1} during spring; $\overline{q}$ = 7 m^3 s^{-1} during autumn). This incongruity in seasonal discharge arises because during spring Mississippi River stage is generally high and a hydraulic gradient sufficient to discharge larger volumes of river water through the diversion structure exists. During autumn, low river stage and the resulting absence of this hydraulic gradient generally prohibit river discharge through the structure. Similar to the dataset analyzed in the previous section, cross-spectral analyses were performed on each three-month time series and then ensemble averaged across the three years.

During spring in the upper estuary, multiple coherence exceeds 0.6 for periods longer than 7 days but gradually diminishes with increasing frequency (Figure 2.5a). River discharge and coastal sea level were both important in forcing upper estuary fluctuations over periods of one week and greater, as shown by the high partial coherences of water level with both inputs across these frequencies. The observed upper estuary spring sea level power spectrum is plotted in Figure 2.5b, along with the cross-

spectral and autospectral terms associated with river discharge and coastal sea level. The variance contained in the autospectral term for river discharge is on the same order as that contained in the autospectral term for remote forcing, indicating that both inputs are important in governing upper estuary sea level variability. A small amount of variability, which cannot be assigned to either forcing input, is contained in the cross-spectral term across periods greater than about one week.

Multiple coherence for the upper estuary during autumn is similar to that in the spring, but the relative contributions to the variance by each forcing function are clearly different (Figure 2.5c). Partial coherence of water level with river discharge generally is less than the 95% significance threshold across all frequencies, while partial coherence of water level with coastal sea level is nearly identical to the multiple coherence of the model, suggesting that upper estuary sea levels during fall are almost entirely coastally-forced. These trends are confirmed by comparing the observed sea level spectrum at the lower estuary location with output spectra coherent with each forcing function (Figure 2.5d), which clearly indicate the spectral response due to freshwater inputs is negligible across all frequencies. The majority of the energy is contained within the autospectral term for coastal forcing, and almost no energy is associated with the cross-spectral term. Although the multiple coherence during both seasons substantially diminishes with increasing frequency, greater than 80% of the subtidal variance in the upper estuary exists at frequencies where multiple coherence exceeds 0.6, suggesting that during both seasons the model adequately describes the first order response at that location.

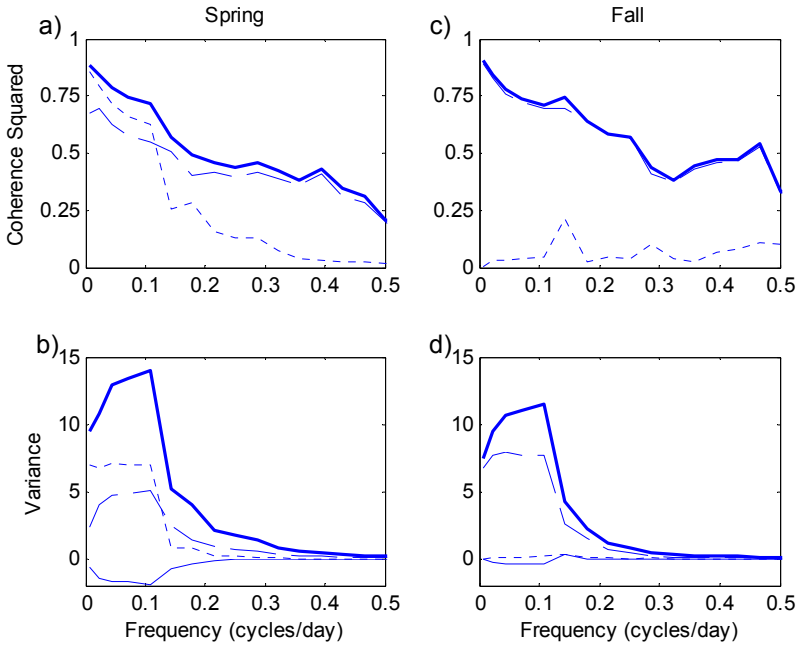

Figure 2.5. (top) Multiple coherence (thick solid line) of η_o and q with upper estuary sea level during spring (a) and fall (c) seasons. Partial coherences of η_o (long, dashed line) and q (dotted line) with upper estuary sea level are also shown. (bottom) Observed upper estuary sea level power spectra (thick, solid line) during spring (b) and fall (d) seasons. Also shown are variance contributions from η_o (long, dashed line) , τ (dotted line), and η_o and τ cross-spectrum (thin solid line).

The amplitude of the transfer function relating freshwater discharge to upper estuary sea level during spring is shown in Figure 2.6a. Across periods of 10 days and greater, the upper estuary sea level response to a 1 m^3 s^{-1} discharge of freshwater from the river diversion structure is between 0.15 and 0.20 cm. The transfer function modulus decreases with increasing frequency, indicating longer duration releases of river water are more effective than shorter releases at creating a marked water level response in the upper estuary. This frequency-dependent nature of the response may exist because considerable time is required for the main conveyance channels downestuary to reach their maximum discharge capacity. Once this capacity is exceeded, additional river inputs are discharged through the estuary as sheet flow over highly-frictional, vegetated

mud flats. After the onset of sheet flow occurs, water level in the upper estuary continues to increase until the pressure resulting from the surface slope equals or exceeds the frictional resistance to flow through marshes and sinuous channels. Because the maximum discharge the river diversion can convey is 225 $m^3 s^{-1}$, results of this analysis suggest that, in the absence of remote atmospheric effects, the maximum expected river-induced water level response in the upper estuary is between 34 and 45 cm. The phase spectrum shows that over periods greater than 10 days, sea level lagged freshwater discharge by 2 to 3 days (Figure 2.6b). The phase relationship between the two variables becomes increasingly less reliable over higher frequencies, owing to the greatly reduced partial coherence between them. The autumn transfer function modulus and phase spectrum are not shown because coherence between the two variables was below the 95% significance level across all frequencies.

Transfer function amplitudes of coastally-generated sea level fluctuations in the upper estuary sea level for autumn and spring are shown in Fig 2.7a. The trend is the same for both seasons, where the amplitude factor approaches 1.0 over very low frequencies, and gradually decreases to 0.2 for fluctuations with periods of 2 days. Although the spring amplitude factor appears to be slightly less than its fall counterpart, the 95% confidence intervals overlap, indicating no difference in response to coastal forcing exists between the two time periods. The shape of the transfer function moduli show that coastal forcing is much more effective at inducing a sea level response in the upper estuary when the coastal fluctuations vary over longer periods. Phase spectra (Figure 2.7b) show that upper estuary sea level fluctuations lag those at the coastal

station, consistent with Ekman convergence at the coast being the dynamical cause of the relationship.

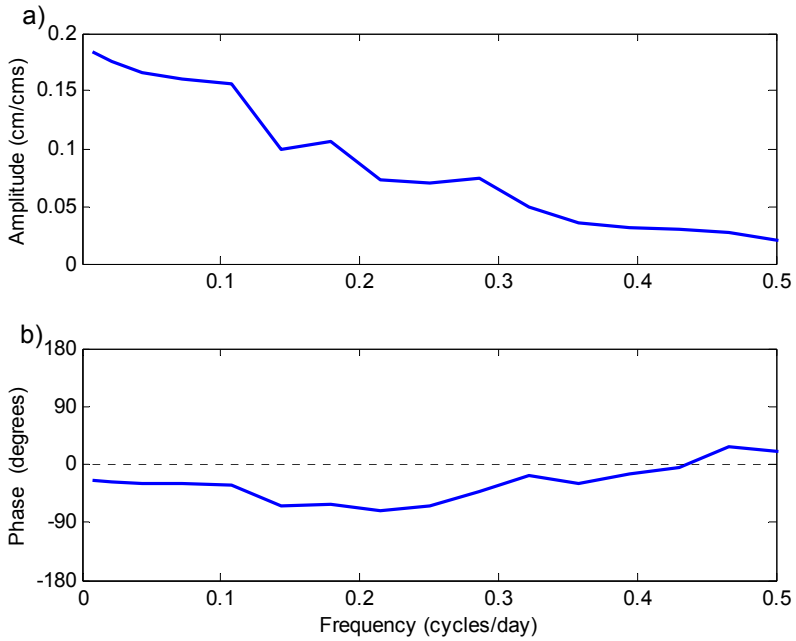

Figure 2.6. Transfer function amplitude (a) and phase (b) between q and upper estuary sea level.

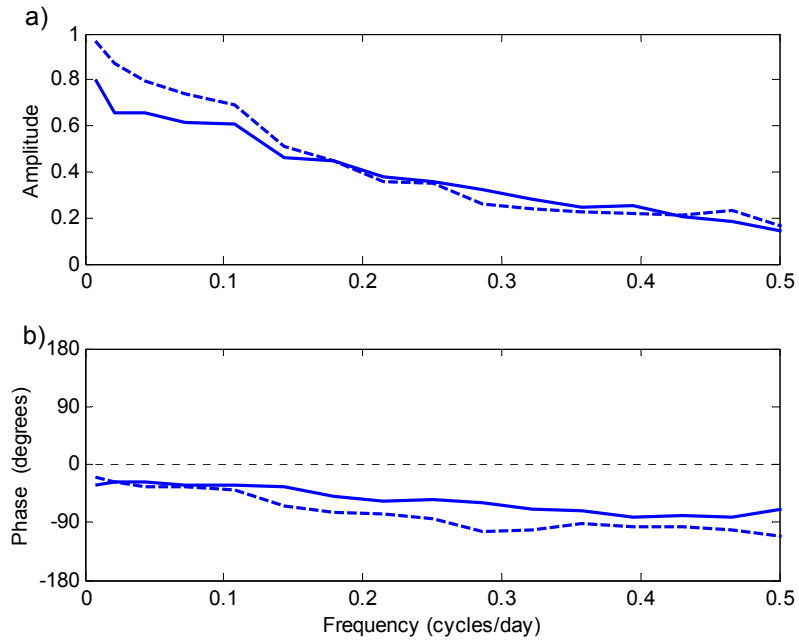

Figure 2.7. Transfer function amplitude (a) and phase (b) between η_o and upper estuary sea level in spring (solid line) and fall (long, dashed line).

Results from the lower estuary site were very similar for both seasons. Multiple coherence generally exceeded 0.8 across all frequencies (Figure 2.8a, c), indicating that the two-input model effectively describes the first-order response at this location. Variability at the lower estuary was almost entirely attributable to coastal sea level fluctuations, as partial coherence between coastal and lower estuary sea levels was generally equal to the multiple coherence (the plot of η_o partial coherence in both seasons is obscured by the multiple coherence line). Partial coherence between freshwater discharge and lower estuary sea level was below the 95% significance level across all subtidal frequencies, indicating that regardless of season, freshwater discharge has no measurable impact on sea level in the lower estuary. Comparison of the lower estuary sea level power spectra with output spectra attributable to the two forcing functions verifies the dominance of coastally-forced fluctuations; variability attributable to the cross-spectral terms are negligible (Figure 2.8b, d).

Amplitude and phase relationships between coastal and lower estuary sea levels are shown in Figure 2.9. The patterns are the same for both seasons, where the transfer function moduli decrease from near unity at very low frequencies to around 0.6 at 0.5 cpd, and estuarine sea level fluctuations lag those that occur at the coast. Comparison between the two sites shows that the amplitude attenuation and phase lag of coastally-forced fluctuations is considerably greater at the upper estuary site. Amplitude and phase relationships between freshwater discharge and lower estuary sea level are not shown because partial coherence between the two variables was insignificant across all frequencies.

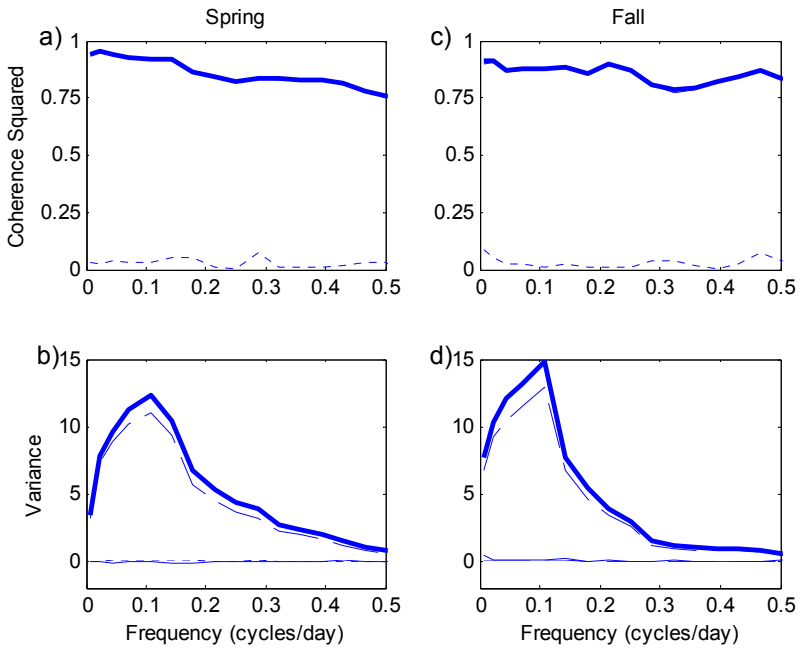

Figure 2.8. (top) Multiple coherence (thick solid line) of η_o and q with lower estuary sea level during spring (a) and fall (c) seasons. Partial coherences of η_o (long, dashed line; obscured by plot of multiple coherence) and q (dotted line) with lower estuary sea level are also shown. (bottom) Observed lower estuary sea level power spectra (thick, solid line) during spring (left) and fall (right) seasons. Also shown are variance contributions from η_o (long, dashed line) , τ (dotted line), and η_o and τ cross-spectrum (thin solid line).

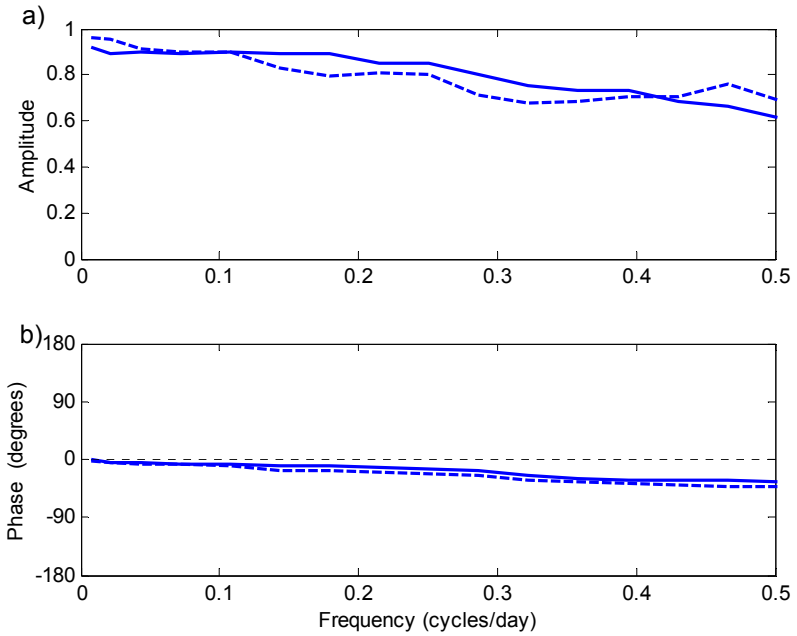

Figure 2.9. Transfer function amplitude (a) and phase (b) between η_o and lower estuary sea level in spring (solid line) and fall (long, dashed line).

Tidal Variations

Least squares harmonic analysis (Dronkers 1964) was performed on hourly sea level time series taken at η_o, η_{lo}, and η_{up} from 28 Jan 1999 to 28 Jan 2000 to obtain amplitude and phase estimates for the K_1, O_1, and M_2 tidal constituents (Table 2.1). At all sites, greater than 88% of the observed tidal variance was accounted for by theses three constituents.

Table 2.1. Amplitude (amp), phase (φ), and percent total tidal variance of major tidal constituents for η_o, η_{lo}, and n_{up}. Phase estimates are relative to η_o.

	O_1			K_1			M_2		
Site	*Amp* (cm)	φ (deg.)	% Var	*Amp* (cm)	φ (deg.)	% Var	*Amp* (cm)	φ (deg.)	% Var
η_o	12.5	0	45.1	12.7	0	46.2	2.3	0	1.5
η_{lo}	7.1	38	42.4	7.8	33	51.2	0.9	54	0.7
η_{up}	0.9	149	42.3	0.9	154	46.0	0.1	214	0.2

Astronomical tides in the Breton Sound estuary are co-dominated by the K_1 and O_1 constituents; variance associated with semi-diurnal constituents is negligible. Strong amplitude attenuation is evident as tidal waves move up the Breton Sound estuary, where the amplitudes of the diurnal constituents decrease from near 12 cm at η_o to approximately 7 cm at η_{lo}, and they are less than 1 cm at η_{up}. Diurnal tides in the upper estuary lag those at the coastal ocean by approximately 150º, which is about 10 h for a signal of diurnal frequency.

Discussion

As shown by the partial coherence analysis of remote and local atmospheric effects in the absence of river forcing during autumn, the remote effect dominates the local effect in forcing water level variability inside the estuary. Direct local wind stress forcing is apparently unimportant inside the system. Instead, wind stress is effective only

over the coastal ocean, where Ekman dynamics force setup and setdown at the marine boundary. This dynamic produces pressure gradients that drive water in and out of the estuary. Exchange can occur either through a multitude of canals and circuitous bayous, or over a vegetated marsh surface as sheet flow when sea level is high enough. Either route is highly frictional when compared with estuary-shelf exchange occurring in deeper, more open embayments such as the Chesapeake or Delaware estuaries. As sea level builds up immediately outside the estuary over the shelf, friction restricts the rate at which water can enter the estuary, causing attenuated fluctuations inside the system that lag those at the marine boundary. The attenuation and phase lag increase upestuary, but the levels do tend to equalize as the period of the coastal oscillations increases. This dynamic is clearly shown in the transfer function amplitudes (Figure 2.7, 2.9). The frictional landscape features thus collectively act to low-pass filter externally generated pressure waves to the extent where coastally-forced water level fluctuations in the upper estuary over tidal timescales are negligible in the upper estuary. Flooding events that are large enough to inundate the vegetated marsh regions in the upper estuary and facilitate materials exchange between the marshes and channelized flow routes, and ultimately export these materials to the coastal ocean are therefore limited to subtidal regions of the frequency spectrum.

The high degree of frictional dissipation of long wave energy combined with the orientation of the estuary can explain the apparent atypical slope response to local wind stress forcing in the Breton Sound estuary. The same landscape features that promote wave energy dissipation also limit fetch, and thus the water level response to local wind stress forcing, inside the system. For this system, axes of along-estuary and along-shore

winds are only offset by about 30°, obscuring the distinction between local and remote wind forcing. Thus, when winds are blowing down estuary, a large upcoast (eastward) component exists, resulting in large, immediate reductions in coastal sea level through Ekman transport. Because friction attenuates and retards the ensuing fluctuations inside the estuary, the onset of downestuary (and largely eastward) winds are associated with coastal sea levels that are lower than those inside the estuary, opposite of what equation (2) would predict the slope response to be in the absence of bottom friction. Examination of partial coherent output spectra obtained from the multiple input linear model allows the estuarine sea-level variability attributable to local wind stress forcing and remote forcing through Ekman set up and set down to be separated, and confirms the dominance of the remote mechanism. Although some energy is contained in the cross-spectral term that cannot reliably be assigned to either of the atmospheric forcing inputs, it is small compared to the disparity of variability that exists between the two autospectral terms.

A one-dimensional frequency-dependent analytical model (Wong 1990) has been used to examine coastally-induced sea-level variability in Long Island Sound and in Delaware Bay (Wong and Moses-Hall 1998; Janzen and Wong 2002). Amplitude and phase spectra can be obtained from the model that relate coastal sea level fluctuations outside the estuary to those at location x inside the estuary, where x is the distance from the estuary mouth. Here the same model is applied to the shallow, deltaic Breton Sound estuary, and the linear drag coefficient (C_D) is tuned to provide model-generated transfer function amplitude and phase spectra that best fit those obtained from cross-spectral analysis of the observations obtained at η_{up} and η_{lo}. To apply the model, we assume the Breton Sound to be uniform in depth (h = 1.5 m), and its length (L) is taken to be 43 km.

Setting C_D equal to 3×10^{-3} m s^{-1} provides model predictions that are in good agreement with the observations at η_{lo} (x = 10 km) and η_{up} (x = 36 km) over much of the subtidal frequency spectrum (Figure 2.10). Comparison of model predictions with normalized amplitudes and phases of the K_1 tidal constituent obtained through harmonic analysis indicates that the analytical model also is effective in describing the response of estuarine sea level to coastal forcing over tidal time scales (Table 2.2).

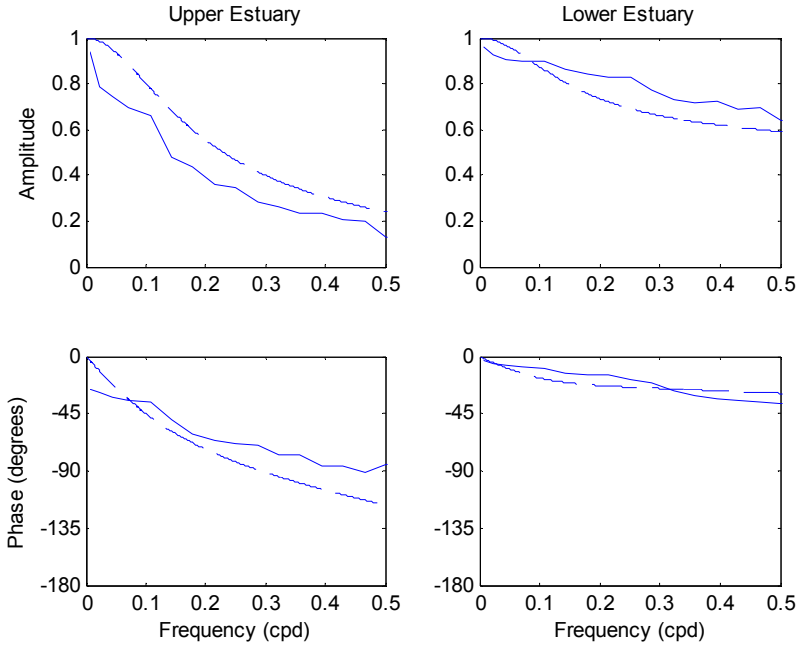

Figure 2.10. Transfer function amplitudes (top) and phase (bottom) spectra of coastally-forced estuarine sea level variability for the upper (left; x = 36 km) and lower (right; x = 10 km) estuary. Estimates obtained from cross-spectral analysis of observations are shown by solid line; model predictions are shown by dashed line.

Table 2.2. Observed and model-predicted tidal amplitudes and phase at n_{up} and η_{lo}, normalized to η_o.

	Normalized Amplitude		Phase	
Location	Observed	Predicted	Observed	Predicted
η_{up}	0.07	0.10	-154	-162
η_{lo}	0.62	0.49	-33	-40

Appropriate parameters for estuarine geometry and the linear drag coefficient (Table 2.3) were selected to obtain model-generated amplitude and phase spectra at two normalized distances (x / L) from the estuary mouth for three relatively deep (h > 8m) east coast estuaries – Long Island Sound, Chesapeake Bay, and Delaware Bay.

Table 2.3. Parameters of mean depth (h), length (L), linear drag coefficient (C_D), natural frequency (ω_n), frictional dissipation frequency (ω_f), and ω_f / ω_r for Breton Sound and other estuaries where dynamics of coastal forcing have been previously investigated.

Estuary	h **(m)**	L **(km)**	C_D **(m s^{-1})**	ω_n **(rad s^{-1})**	ω_f **(rad s^{-1})**	ω_f / ω_n	**Source**
Long Island Sound	22.0	150	1.1×10^{-3}	9.8×10^{-5}	5.0×10^{-5}	0.5	Wong, 1990
Chesapeake	8.4	270	1.0×10^{-4}	3.3×10^{-5}	1.3×10^{-5}	0.5	Wang, 1979
Delaware	10.0	215	1.0×10^{-3}	4.6×10^{-5}	1.0×10^{-4}	2.2	Janzen and Wong, 2002
Breton Sound	1.5	43	3.0×10^{-3}	8.8×10^{-5}	2.0×10^{-3}	22.7	this study

These normalized distances correspond to η_{lo} (x / L = 0.30) and η_{up} (x / L = 0.84) in the Breton Sound estuary, which allow for comparisons to be made across the systems (Figure 2.11). In the deeper, pelagic systems coastally-forced variations show very little attenuation, or even amplification resulting from resonance at some frequencies. Resonance in estuarine basins having free communication with the coastal ocean tends to occur when the ratio of the forcing frequency ω to the natural frequency ω_n approaches π/2, 3 π/2, 5 π/2, …, etc. (Wong 1990), unless it is countermanded by sufficient frictional damping. Coastally-forced variations in Breton Sound, on the other hand, show intense frictional attenuation at tidal frequencies, and the attenuation extends well into the subtidal frequencies. This attenuation occurs because the frequency of frictional decay,

$\omega_f = C_D / h$, is more than 20 times greater than ω_n. This ratio (ω_f / ω_n) is at least an order of magnitude less in other systems examined with the analytical model (Table 2.3), where frictional effects were observed to be much less severe.

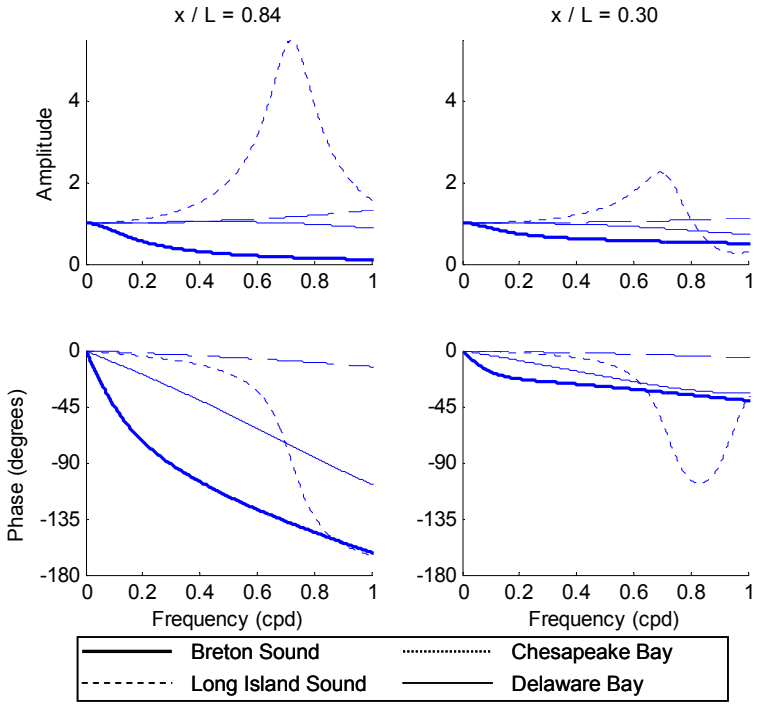

Figure 2.11. Transfer function amplitude (top) and phase (bottom) spectra of coastally-forced estuarine sea-level variability predicted by the frequency-dependent analytical model for the Breton Sound, Long Island Sound, Chesapeake, and Delaware estuaries. Spectra are shown for two normalized distances from the estuary mouth (x / L) – 0.8 (left) and 0.3 (right).

The data show that, in the absence of freshwater inputs, sea level variability in the entire system is almost entirely driven by co-oscillations between the estuary and the adjacent shelf that are forced by along-shelf winds. The situation changes during spring, when substantial quantities of river water are discharged into the system at the head of the estuary. As shown by the coherent output spectra, during this time period, upper estuary sea level variability attributable to freshwater discharge is on the same order as variability forced by coastal oscillations. The 30 to 45 cm maximum upper estuary water

level response to discharge through the river diversion indicated by the transfer function suggests that, at least in the upper estuary, the river diversion has the capacity to induce high stages and subsequent sheet flow necessary to deliver fluvial materials to the marsh interior. The fact that partial coherence between freshwater discharge and sea level diminishes to insignificant levels in the lower estuary suggests that the impact area of the river diversion in terms of water level response extends somewhere between 7 and 33 km (the distance between the upper and lower locations) downestuary from the structure. It also is consistent with results from studies investigating sedimentation trends associated with the freshwater diversion, which indicate that deposition associated with diversion-induced overland flow was primarily limited to within 6 to 10 km of the freshwater diversion structure (Wheelock 2003).

The Mississippi River deltaic plain is an excellent setting to further explore aspects of estuarine subtidal variability, and the Breton Sound estuary is one of several estuarine systems situated along the deltaic plain. While all of these systems are deltaic in nature and likely are highly frictional with regard to long wave propagation, they differ markedly in other respects such as how they communicate with shelf waters. Deltaic estuaries can also differ largely in the relative amounts of river and coastal forcing they receive. Both of these mechanisms can induce overbank flooding and overland flow in deltas, but with fundamentally different effects on the landscape; river forcing is generally associated with delivery and subsequent deposition of allocthonous sediments and delta progradation, while coastal forcing is generally associated with tidal scour, erosion and marine transgression (Madden et al 1988; Roberts 1997). Thus, to clearly understand the effect that flooding has on the deltaic landscape, it is important to

distinguish sources of inundation. Because deltaic systems comprise a substantial portion of the world's estuaries, the relative roles of river and coastal forcing in these systems deserve further investigation.

Literature Cited

Bendat, J.S. and A.G. Piersol. 1993. Engineering Applications of Correlation and Spectral Analysis, Second Edition, Wiley, New York.

Bloomfield, P. 1976. Fourier Analysis of Time Series: An Introduction, John Wiley, New York.

Coleman, J.M., H.H. Roberts, and G.W. Stone. 1998. The Mississippi River delta: an overview. Journal of Coastal Research 3: 698-716.

Current, C. L. 1996. Spectral model simulation of wind driven subinertial circulation on the inner Texas-Louisiana Shelf. Ph.D. dissertation, Texas A&M University, College Station, TX.

Dronkers, J.J. 1964. Tidal Computations in Rivers and Coastal Waters. North-Holland Publishing Company, Amsterdam.

Elliott, A.J. and D.P. Wang. 1978. The effect of meteorological forcing on the Chesapeake Bay: the coupling between and estuarine system and its adjacent coastal waters. In: Hydrodynamics of Estuaries and Fjords (ed. J.C.J. Nihoul), Elsvier Scientific Pulb. Co., Amsterdam, pp 127-145.

Filadelfo, R., R.E. Wilson, and E. Gomez-Reyes. 1991. Subtidal Eulerian currents in the upper and lower East River tidal straight: spring 1981. Journal of Geophysical Research 96: 15217-15226.

Garvine, R.W. 1985. A simple model of estuarine subtidal fluctuations forced by local and remote wind stress. Journal of Geophysical Research 90:11945-11948.

Garvine, R.W., R.K. McCarthy, and K.C. Wong. 1992. The axial salinity distribution in the Delaware estuary and its weak response to river discharge. Estuarine, Coastal and Shelf Science 35: 157-165.

Iseri, K.T. and W.B. Langbein. 1974. Large rivers of the United States. U.S. Geological Survey Circular 686, U.S. Geological Survey, Reston, Virginia

Janzen, C.D. and K.C. Wong. 1998. On the low-frequency transport processes in a shallow coastal lagoon. Estuaries 21: 754-756.

Janzen, C.D. and K.C. Wong. 2002. Wind-forced dynamics at the estuary-shelf interface of a large coastal plain estuary. Journal of Geophysical Research 107 (C10), 3138, doi:10.1029/2001JC000959.

Jenkins, G.M. and D.G. Watts. 1998. Spectral Analysis and its Applications, Fifth Edition. Emerson-Adams Press, Boca Raton, FL.

Large, W.G. and S. Pond. 1981. Open ocean momentum flux measurements in moderate to strong winds. Journal of Physical Oceanography 11: 324-336.

Madden, C.J., J.W. Day, Jr., and J.M. Randall. 1988. Freshwater and marine coupling in estuaries of the Mississippi River deltaic plain. Limnology and Oceanography 33**:** 982–10004.

Marmer, H.A. 1954. Tides and sea level in the Gulf of Mexico. Fishery Bulletin of the Fish and Wildlife Service 89: 101-118.

Noble, M.A., W.W. Schroeder, W.J. Wiseman, Jr., H.F. Ryan, and G. Gelfenbaum. 1996. Subtidal circulation patterns in a shallow, highly stratified estuary: Mobile Bay, Alabama. Journal of Geophysical Research 101:25689-25703.

Pritchard, D.W. 1955. Estuarine circulation patterns. Proceedings of the American Society of Civil Engineers 81, No. 717.

Roberts, H.H. 1997. Dynamic changes of the Holocene Mississippi River delta plain: The delta cycle. Journal of Coastal Research 13: 605-627.

Schroeder, W.W., W.J. Wiseman, Jr. and S.P. Dinnel. 1990. Wind and river induced fluctuations in a small, shallow, tributary estuary. In R. T. Cheng, (ed.), Residual Currents and Long Term Transport. Springer-Verlag, New York, pp.481-493

Stern, M.K., J.W. Day, Jr., and K.G. Teague. 1991 Nutrient transport in a riverine-influenced tidal freshwater bayou in Louisiana. Estuaries 14: 382–394.

Wang, D.P. 1979. Subtidal sea level variations in the Chesapeake Bay and relations to atmospheric forcing. Journal of Physical oceanography 9: 413-421

.

Weisberg, R.H. 1976. The nontidal flow in the Providence River of Narragansett Bay: a stochastic approach to estuarine circulation. Journal of Physical Oceanography 6: 721-934.

Wheelock, K.W. 2003. Pulsed river flooding effects on sediment deposition in Breton Sound Estuary, M. S. thesis, Louisiana State University, Baton Rouge, LA,.

Wong, K.C. 1990. Sea level variability in Long Island Sound. Estuaries 13: 362-372.

Wong, K.C. 1995. On the relationship between long-term salinity variations and river discharge in the middle reach of the Delaware Estuary. Journal of Geophysical Research 100: 20705-20713.

Wong, K.C. and J. DiLorenzo. 1988. The response of Delaware's inland bays to ocean forcing. Journal of Geophysical Research 93: 12525-12535.

Wong, K.C and R.W. Garvine. 1984. Observations of wind-induced, subtidal variability in the Delaware Estuary. Journal of Geophysical Research 89: 10589-10597.

Wong, K.C and J.E. Moses-Hall. On the relative importance of the remote and local wind effects to the subtidal variability in a coastal plain estuary. Journal of Geophysical Research 89: 18393-18404.

CHAPTER III.

SEDIMENT LOADING INTO A SUBSIDING LOUISIANA DELTAIC ESTUARY THROUGH A MISSISSIPPI RIVER DIVERSION

Introduction

A principal determinant in the structure and function of riparian landscapes is the flood pulse (Junk et al. 1989). In large river deltas, pulsing events occur on a broad range of spatial and temporal scales, ranging from very large delta switching events that occur every thousand years to daily tides (Day et al. 1995). Intermediate to these pulses are annual river floods and meteorological tides that help nourish naturally subsiding deltaic landscapes with nutrients and mineral sediments (Hensel et al. 1998; Reed 1989). In addition to introducing large amounts of fluvial materials to estuarine environments, pulsed events also can cause widespread flooding and facilitate materials exchange between pelagic and riparian zones.

Eustatic sea level rise (ESLR), defined as an increase in sea level resulting from a change in ocean volume, estimated to be 1 to 2 mm yr^{-1} (IPCC 2001), is a critical problem facing coastal regions today. The problem is greatly exacerbated in subsiding deltas worldwide, where subsidence contributes to a relative sea level rise (RSLR; an apparent change in local sea level due to the additive effects of ESLR and subsidence) that far exceeds ESLR alone. Water withdrawals upstream of the Nile delta have accelerated the erosion of the promontories situated at the two river mouths (Sestini 1992) and contributed to RSLR rates exceeding 5 mm yr^{-1} (Stanley 1990). In the Po delta, RSLR rates of 1 to 3 mm yr^{-1} are reported, largely attributable to reductions in hydrostatic pressure associated with wetland reclamation for agricultural use (Carbognin et al. 2004). Municipal groundwater extraction along the Yangtze River has created one

of the fastest subsiding deltas worldwide, with RSLR rates approaching 12 mm yr^{-1} (Xiqing 1998).

Relative sea level rise can result in increased frequency and duration of marsh flooding and contribute to higher mean salinities. Together, these effects can stress local plant communities (Mendelssohn and McKee 1988; McKee and Mendelssohn 1989), and decrease belowground production necessary to strengthen sediment infrastructure and combat wave and current erosion of tidal mud flats. Over long timescales, these circumstances can result in the conversion of large expanses of vegetated coastal wetlands into open water habitats, resulting in coastal land loss, a crisis seen in coastal regions around the globe

Rates of RLSR in excess of 10 mm yr^{-1} (approaching those of the Yangtze) have been observed in some regions of the Mississippi River delta (Coleman et al. 1998). Pulsed fluvial inputs to the delta have been virtually eliminated for nearly a century due to its hydrologic separation from the Mississippi River by containment levees. Additionally, the construction of oil and gas pipeline canals has resulted in increased flooding stemming from impoundment effects associated with deposition of dredge spoil along the canal banks, as well as increasing tidal energy and salinity through enhanced estuary-ocean exchange (Turner 1997). Although the relative importance of these impacts remains unclear, this suite of anthropogenic impacts has contributed to a situation where statewide wetland loss rates have approached 115 km^2 yr^{-1} (Barras et al. 1994). Severe decreases in fisheries production (Thomas 1999), storm surge protection, and an extensive failure of minerals extraction infrastructure are expected to result from the landscape change, if it continues to occur unchecked for the next several decades

(Coast 2050 1998). As part of a large scale restoration program to ameliorate this situation, controlled river diversions designed to reconnect the coastal wetlands of the deltaic plain with the Mississippi River have been constructed. In addition to reducing saltwater intrusion and nourishing wetland communities with nutrients, it is widely held that deposition of mineral sediments delivered by river diversions onto subsiding marshes can help offset RSLR.

Most existing river diversions in Louisiana are designed to regulate estuarine salinities for optimal shellfish production (Coast 2050 1998), and consequently, constraints on freshwater discharge through the diversions often exist when estuarine salinities are low. To more effectively plan and operate freshwater diversion projects for coastal restoration, aspects of their sediment loading potential need to be better understood. Considerable temporal variability in Mississippi River sediment concentration exists and has been positively correlated with river discharge (Mossa 1988; Mossa 1996), thus suggesting that sediment loading into receiving basins may be governed not only by the volume of river water diverted, but also by the timing of the events.

This study examines the response of a deltaic estuary to pulsed introductions of fluvial materials through a controlled diversion structure. The objectives of this study are to 1) quantify and examine temporal variability in sediment loading rates into the Breton Sound estuary from the Mississippi River, and 2) characterize the magnitude and temporal variability in sheet flow response in the upper estuary to fluvial inputs and how they relate to potential sediment loading to the subsiding marshes.

Study Site

The Breton Sound estuary is located approximately 20 km southeast of New Orleans, Louisiana, at the head of the Breton Sound estuary (Figure 3.1). The estuary is 40 km in length and angles southeast toward the Gulf of Mexico. It is bound to the northeast by spoil banks associated with a commercial navigation canal, and on the southwest by the levee of the Mississippi River. The system consists of a foundation of pro-delta clay deposits over which a matrix of fresh, brackish, and saline marshes, barrier islands, natural levees, and former distributary channels of the Mississippi is situated (Coleman et al. 1998). Vegetation communities are dominated by *Spartina patens* in the upper estuary, with a gradual downestuary transition to *S. alternaflora* downestuary, owing to higher salinities and more flooding. Diurnal tide amplitudes are around 14 cm in the lower estuary, but amplitudes in the upper estuary are an order of magnitude less, owing to severe energy dissipation as the tide progresses up the estuary through the highly frictional deltaic landscape (Chapter 2). During autumn and winter, cold front passages occur every 4 to 7 days (Chuang and Wiseman 1983), and amplitudes of coastal water level fluctuations associated with such events typically exceed those forced by astronomical tides. Average annual precipitation at New Orleans is approximately 150 cm.

The Caernarvon Freshwater Diversion structure is located at Mississippi River mile 81.5 above Head of Passes, and is designed to convey water through the river's east containment levee into an outflow channel which discharges the river water into the upper reaches of the Breton Sound estuary. Discharge through the structure, which consists of five 4.6-m gated box culverts, is gravity-driven and generally can occur only

when Mississippi River stage at the Carrollton gauging station in New Orleans exceeds about 1.2 m NAVD 88, although this threshold can vary slightly depending on ambient water levels in the estuarine receiving basin. The structure is designed to discharge up to 225 $m^3 s^{-1}$ of Mississippi River water. Average monthly total suspended sediments (TSS) concentrations in surface waters of the Mississippi River vary from 15 mg L^{-1} in September to 130 mg L^{-1} in February (Figure 3.2). Grain size analysis conducted on water samples collected in the outflow channel during March 2003 showed a particle size distribution of 63% silt, 36% clay, and 1% sand.

When diversion discharge is less than about 100 $m^3 s^{-1}$, nearly 99% of diverted river water flows downestuary through two dominant channelized flow routes: an east route consisting of Bayous Mandeville and Terre aux Boeufs, and a west route through Delacroix Canal and Oak River (Figure 3.1). In situations where diversion discharge exceeds the summed conveyance capacity of the east and west flow routes, river water overbanks and traverses the vegetated marsh as sheet flow. This dynamic can be modified by wind stress, where winds blowing from the southeast tend to accumulate Gulf of Mexico waters in the seaward end of the estuary, reducing the hydraulic gradient between the upper and lower ends of the system (Chapter 2). This circumstance has the overall effect of reducing the conveyance capacity of the two major flow routes and thus decreasing the threshold diversion discharge necessary to induce sheet flow over the upper estuary. The reverse occurs for winds blowing from the north or west, when greater diversion discharge is necessary to induce overland flow, because the along-estuary sea level gradient is greater, which enhances export of fluvial inputs from the

estuary. Overall, the hydrodynamics of the system are controlled by prevailing winds and pulsed fluvial inputs (Chapter 2).

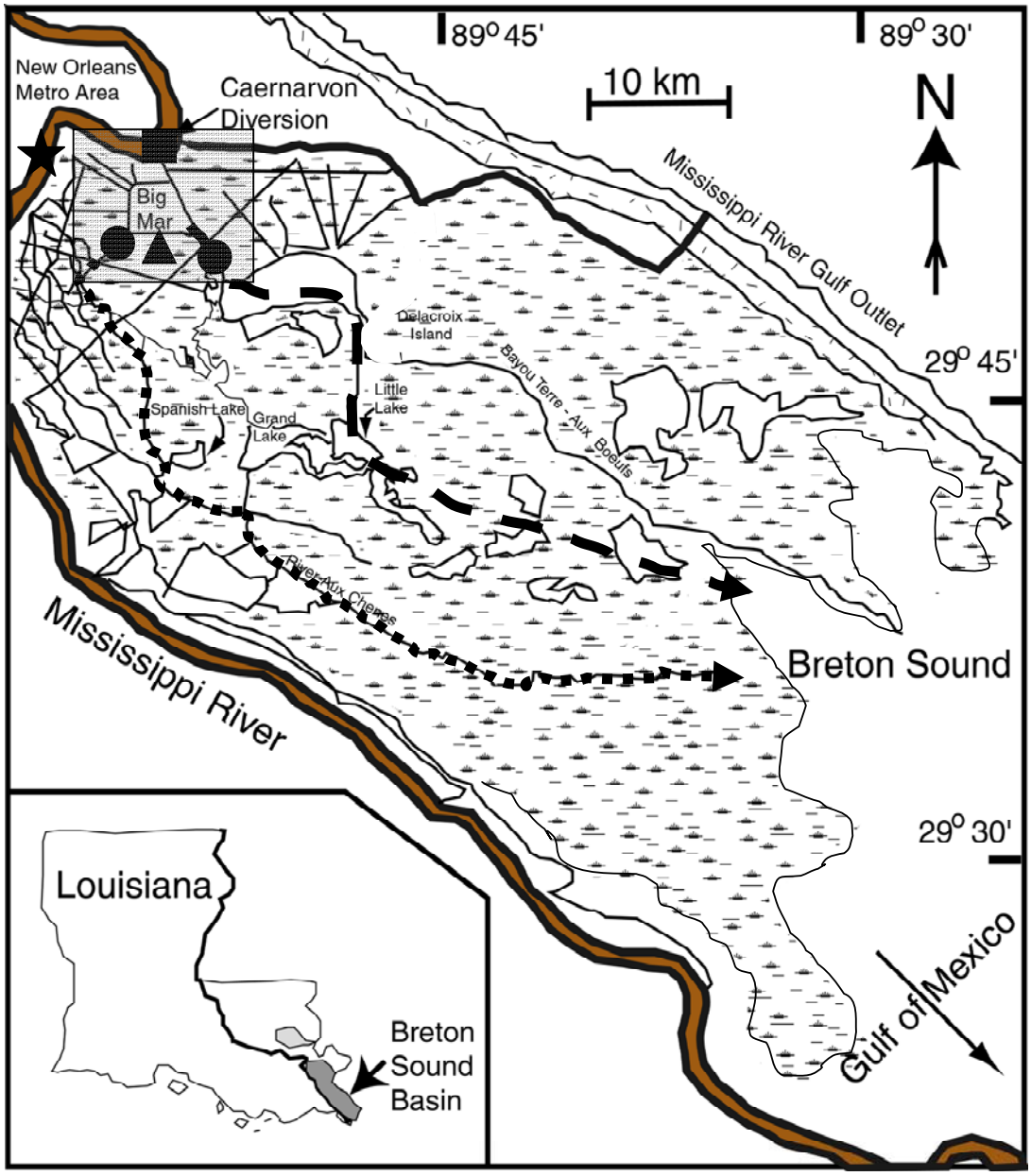

Figure 3.1. Map of the study area showing locations of the river diversion structure (square), hourly discharge stations in the upper reaches of the eastern and western flow routes (circles), the marsh water level station (triangle) and location where TSS concentrations in the Mississippi River were sampled (star). The eastern and western channelized flow routes are shown by the dashed, arrowed lines. The upper estuary, where the instrumentation was deployed, is highlighted by the gray shaded box..

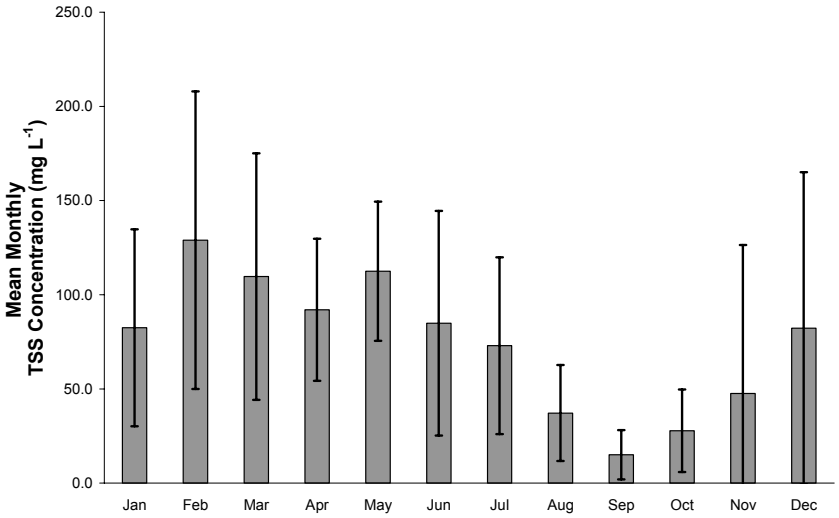

Figure 3.2. Mean monthly TSS concentrations of Mississippi River surface water taken at Belle Chase, LA, from 1991 to 2004. Error bars represent standard deviation.

Materials and Methods

Hourly estimates of discharge were made by the U.S. Geological Survey Water Resources Division in the outflow channel of the diversion structure and in the upper reaches of the eastern and western flow routes (Figure 3.1) from 28 Jan 2002 to Jan 28 2004. These estimates were obtained through a combination of periodic instantaneous (synoptic) discharge measurements recorded with a 600-kHz boat-mounted acoustic Doppler current profiler (RDInstruments™), hourly water level recorded with a pressure transducer (YSI™ 6920), and hourly point measurements of current velocity recorded with a logging acoustic Doppler velocity meter (SonTek™ Argonaut SL). A relationship between the instantaneous discharge and the hourly recorded water level and current velocity was used to compute estimates of hourly discharge at each site (Morlock 2001).

Turbidity of diverted Mississippi River water in the outflow channel was measured hourly with a logging optical backscatter nephelometric turbidity probe (YSI™ 600 OMS), which was field-serviced and calibrated monthly. During the two years of

routine probe servicing, 47 periodic water samples were obtained from 1 m below the water surface and subsequently analyzed for TSS by filtering 100 to 250 mL of each sample through pre-rinsed, pre-ashed, pre-weighed 47 mm GF/F glass microfiber filters. Filters were dried for 24 hours at 105°C, then combusted for 1 hour at 550ºC and weighed. Regression analysis showed the presence of a significant relationship ($p < 0.001$; $r^2 = 0.84$; Figure 3.3) between TSS concentrations obtained from water samples and simultaneously recorded turbidity values. The range of turbidity values used in the regression analysis covered nearly the entire range of values recorded by the probe during the two year study. These findings indicate turbidity measurements adequately captured the temporal variability in TSS concentrations in the outflow channel and reliably predicted suspended sediment concentrations present in diverted Mississippi River water.

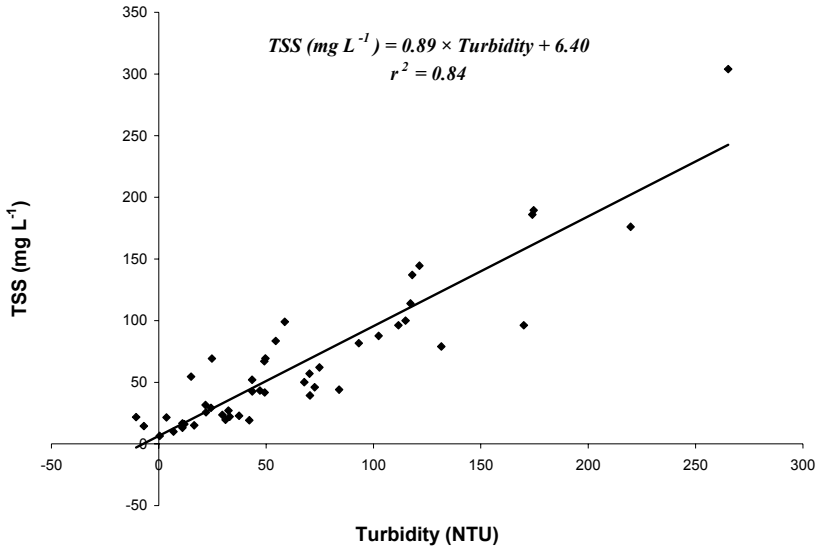

Figure 3.3. Relationship between turbidity measured with optical backscatter probes and TSS concentrations obtained from surface water samples ($n = 47$) in the outfall channel immediately downstream of the river diversion.

To assess the reliability of using turbidity at a single point in the outflow channel as an indicator of TSS concentrations throughout the channel's entire cross section, TSS

concentrations were determined from water samples obtained at four depths along five equally-spaced vertical transects across the channel. This procedure was performed 5 times across diversion discharge conditions ranging from 0 $m^3 s^{-1}$ to 185 $m^3 s^{-1}$. In general, TSS concentrations were slightly greater near the bottom of the channel, but overall, the coefficient of variation in concentrations along the vertical axis did not exceed 20% (Table 3.1). Horizontal variations across the channel showed no obvious spatial pattern, and the coefficient of variation along this axis was below 10% during all sampling events. Together, these data indicate that TSS variability throughout the cross-section was low, and suggest that turbidity data collected at a single point in the channel provided reasonable estimates of TSS concentrations throughout the outflow channel.

Table 3.1. Mean TSS concentrations in the diversion outfall channel, with cross-channel (CV_x) and vertical (CV_z) coefficients of variation. Data were obtained by sampling a cross-sectional grid consisting four depths situated across 5 cross-channel locations.

Date	Diversion Discharge ($m^3 s^{-1}$)	Mean TSS ($mg L^{-1}$)	CV_x	CV_z
1/23/2002	0	30.8	4.3	8.0
2/7/2002	185	194.6	2.6	4.1
2/28/2002	15	51.1	8.3	17.7
3/14/2002	185	46.5	2.8	8.0
4/10/2002	15	70.4	4.3	16.2

Instantaneous flux of Mississippi River sediments into the estuary via the diversion structure ($flux_{sed}$) was then computed as

$$flux_{sed} = q_{div} \times tss \quad \textbf{(3.1)}$$

where q_{div} and *tss* are the volume discharge and suspended sediment concentrations in the outflow channel, respectively. Total sediment delivery Q over a time interval *0-T* was determined as

$$Q = \int_0^T flux_{sed} dt \quad \textbf{(3.2)}$$

where t is time.

The volume of diverted river water that bypassed the east and west flow routes and instead was conveyed down the estuary over the marsh surface as sheet flow (q_{resid}) was estimated as

$$q_{resid} = q_{div} - (q_{east} + q_{west}) \quad \textbf{(3.3)}$$

where q_{div} is the discharge of river water entering the estuary at the diversion, and q_{east} and q_{west} are the measured discharges at the upper reaches of the east and west flow routes, respectively. It is important to note that q_{resid} does not indicate specifically where sheet flow is occurring; it simply quantifies the volume of diverted river water not passing the current meters in the upper reaches of the two primary channelized flow routes, which convey nearly all diverted river water to the lower estuary when structure discharge is less than about 100 $m^3 s^{-1}$. Marsh water level was measured hourly in the upper estuary (Figure3.1) to determine if periods of elevated water levels over the marsh coincided with pulsed diversion events and periods when q_{resid} was high.

In addition to these data, monthly values of Mississippi River near surface TSS concentrations approximately 6 km downstream from the Caernarvon freshwater diversion were provided by the Louisiana Department of Environmental Quality. Although considerable vertical variability in TSS concentrations can exist in the river, the diversion structure discharges primarily near surface Mississippi River water; thus

surface TSS concentrations in the river were most relevant for this study. Daily Mississippi River discharge data were obtained at Tarbert Landing, LA (river mile 306), by the U.S. Army Corps of Engineers.

Results

Sediment Loading

Annual sediment delivery through the river diversion during both years of the study was 1.0 to 1.3 × 10^5 metric tons. The temporal pattern was similar during both years, with greatest amounts of delivery occurring between December and March (Figure 3.4). Sediment loading during these months accounted for 88% of the total annual delivery during the two year study.

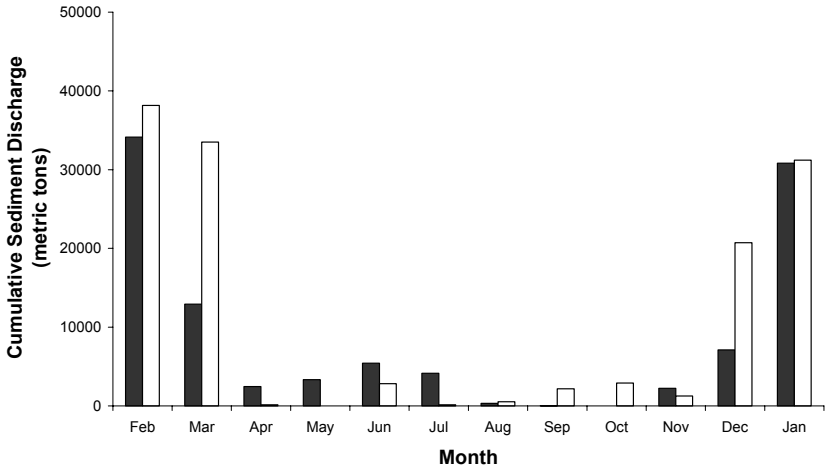

Figure 3.4. Monthly sediment delivery through the diversion structure. Black bars represent values for the first year of the study (Feb 2002 to Jan 2003); white bars represent values for the second year (Feb 2003 to Jan 2004).

Similar seasonal patterns in diversion discharge existed during both years (Figure 3.5a): the occurrence of two pulsed river diversions (shaded boxes) lasting approximately two weeks each during late winter to early spring, little or no discharge during the middle of the year, and increased discharge toward the end of the year.

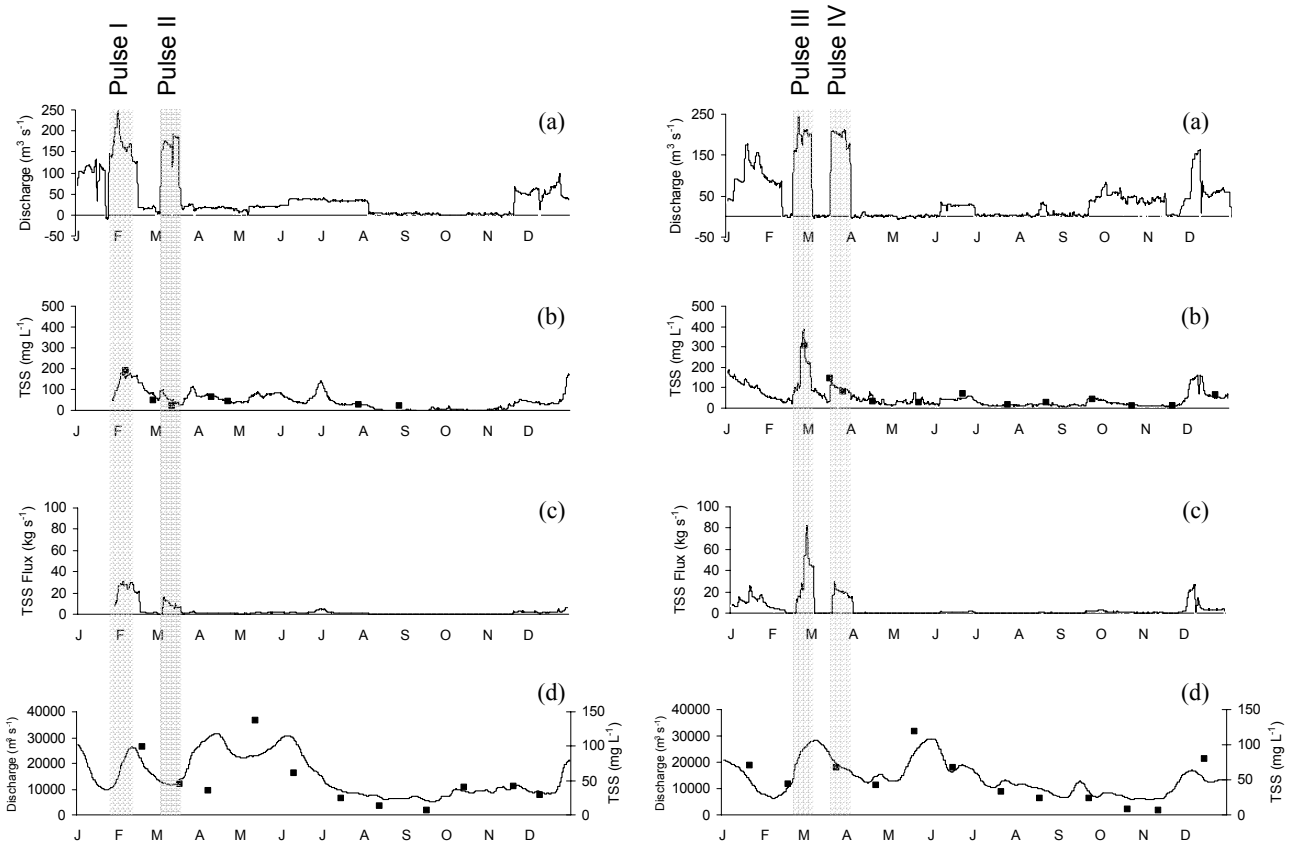

Figure 3.5. Time series of diversion discharge (a), TSS concentrations in the diversion outfall channel estimated with turbidity probe (line) and obtained through laboratory analysis of discrete water samples (squares; b), sediment flux through the river diversion (c), and Mississippi River discharge (line) and river TSS concentrations (squares; d) obtained from surface water samples at Belle Chase, LA for 2002 (left) and 2003 (right). The shaded boxes indicate periods when pulsed diversions occurred

Though the target discharge during each of the pulsed diversions was 185 $m^3 s^{-1}$, controlling discharge through the diversion is not precise, and the observed discharge often exceeded that value. Maximum TSS concentrations of river water in the diversion outflow channel approached 400 mg L^{-1} on one occasion, but generally did not exceed 200 mg L^{-1} (Fig 3.5b). Although minimum TSS concentrations during diversion events were sometimes as low as 10 mg L^{-1}, TSS concentrations of introduced river water generally exceeded 30 mg L^{-1}. Considerable variability in hourly TSS concentrations of diverted river water existed across the four pulsed diversion events, where concentrations range between 30 mg L^{-1} and 400 mg L^{-1}. Time series of sediment flux into the estuary are highly variable, ranging from 0 kg s^{-1} when the diversion structure is closed, to over 80 kg s^{-1} during pulse III (Figure 3.5c).

The high degree of variability in sediment delivery among the pulsing events with similar diversion discharges demonstrates that sediment loading to the Breton Sound estuary is governed not only by the magnitude of the diversion, but also by TSS concentrations in the Mississippi River. Monthly surface samples obtained from Mississippi River water collected at Belle Chase show that considerable temporal variability in TSS concentrations exists in the water diverted into the Breton Sound estuary, and in general, high river TSS concentrations are associated with periods of high river discharge (Figure 3.5d). Following Mossa (1988; 1996) a significant quadratic power relationship was found to exist between the $\log_{10}$ transforms of these two variables ($p < 0.001$; $r^2 = 0.76$; Figure 3.6) obtained from monthly samples spanning 1991-2005. This trend indicates that river TSS concentrations increase with river flow until very high discharges are reached, at which point additional river discharge results in minimal

increases in TSS concentrations. The positive relationship between river discharge and river TSS concentration over the normal discharge range of the river indicates that daily values in river discharge may be used as a proxy for concentrations of sediment suspended in the river.

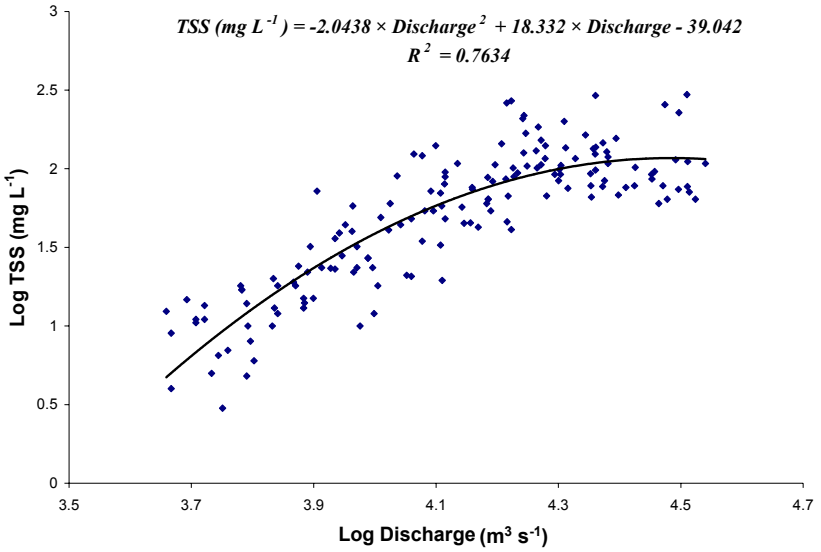

Figure 3.6. Log-log relationship between Mississippi River discharge and TSS concentrations in surface water samples (n = 158) obtained at Belle Chase, LA, from 1991-2004.

Total sediment delivered during pulse I exceeded that of pulse II by a factor of 2.7 (Table 3.2), even though mean diversion discharge during each event was similar. Mean Mississippi River discharge was 20300 m^3 s^{-1} and 12200 m^3 s^{-1} during pulses I and II, respectively, implying that TSS concentrations in the river during pulse I exceeded those during pulse II. This pattern is reflected in the average TSS concentrations of diverted river water measured in the outflow channel, where average hourly values for pulse I far surpassed those of pulse II. During the second year of the study, pulse III delivered nearly twice as much sediment to the Breton Sound estuary as pulse IV, with outfall channel mean TSS concentrations of 197 mg L^{-1} and 100 mg L^{-1} for pulses III and IV,

Table 3.2. Summary statistics for the four pulsed diversion events.

Event	Date	Average Diversion Discharge ($m^3 s^{-1}$)	Duration (d)	Average River Discharge ($m^3 s^{-1}$)	Average TSS (mg L^{-1})	Total Sediment Delivery (metric tons)	Metric tons day^{-1}
Pulse 1	28 Jan – 11 Feb 2002	180	14	2.04×10^4	143	3.02×10^4	2.16×10^3
Pulse 2	04 Mar – 17 Mar 2002	166	14	1.22×10^4	57	1.13×10^4	0.81×10^3
Pulse 3	18 Feb – 03 Mar 2003	195	13	1.97×10^4	197	4.38×10^4	3.29×10^3
Pulse 4	17 Mar – 31 Mar 2003	193	15	2.01×10^4	101	2.46×10^4	1.64×10^3
Mean		184	14	1.81×10^4	125	2.75×10^4	1.98×10^3

respectively. However, mean Mississippi River discharge during these two events was similar (~20000 $m^3 s^{-1}$; Table 3.2), with the only clear difference being that pulse III occurred during the rising limb of a river flood event and pulse IV coincided with the falling limb of the same event (Figure 3.5d). Together, these data show that diversions occurring when river discharge was greater than 20000 $m^3 s^{-1}$ (a discharge that corresponds to bankfull stage conditions in the lower Mississippi River) delivered water into the Breton Sound estuary with TSS concentrations in excess of 100 mg L^{-1}. TSS concentrations of diverted river water were further enhanced when diversions occurred on the rising limbs of such events.

Sheet Flow Response to Diversion

Coincident with the four pulsed diversion events were periods of large residual discharge (Figure 3.7a, b), indicating that a substantial portion of fluvial inputs bypassed the current meters at the upper reaches of the east and west channelized flow routes as it advanced to the Gulf of Mexico. Concurrent with these periods of high residual discharge were episodes of elevated water level over the marsh surface (Fig 3.7c). Taken together, these results indicate that the residual flow in the upper estuary water budget (q_{resid}) may have been attributed to sheet flow over the marsh surface when the conveyance capacity of the channels is exceeded during pulsed diversions.

Considerable short-period (< 5d) variability, likely attributable to wind forcing, is apparent in the residual discharge time series. It is thus instructive to examine the mean distribution of diversion discharge conveyed downestuary through the various routes over longer time periods where opposing wind effects tend to cancel out (Figure 3.8). The selected time periods correspond with time spans of relatively constant diversion

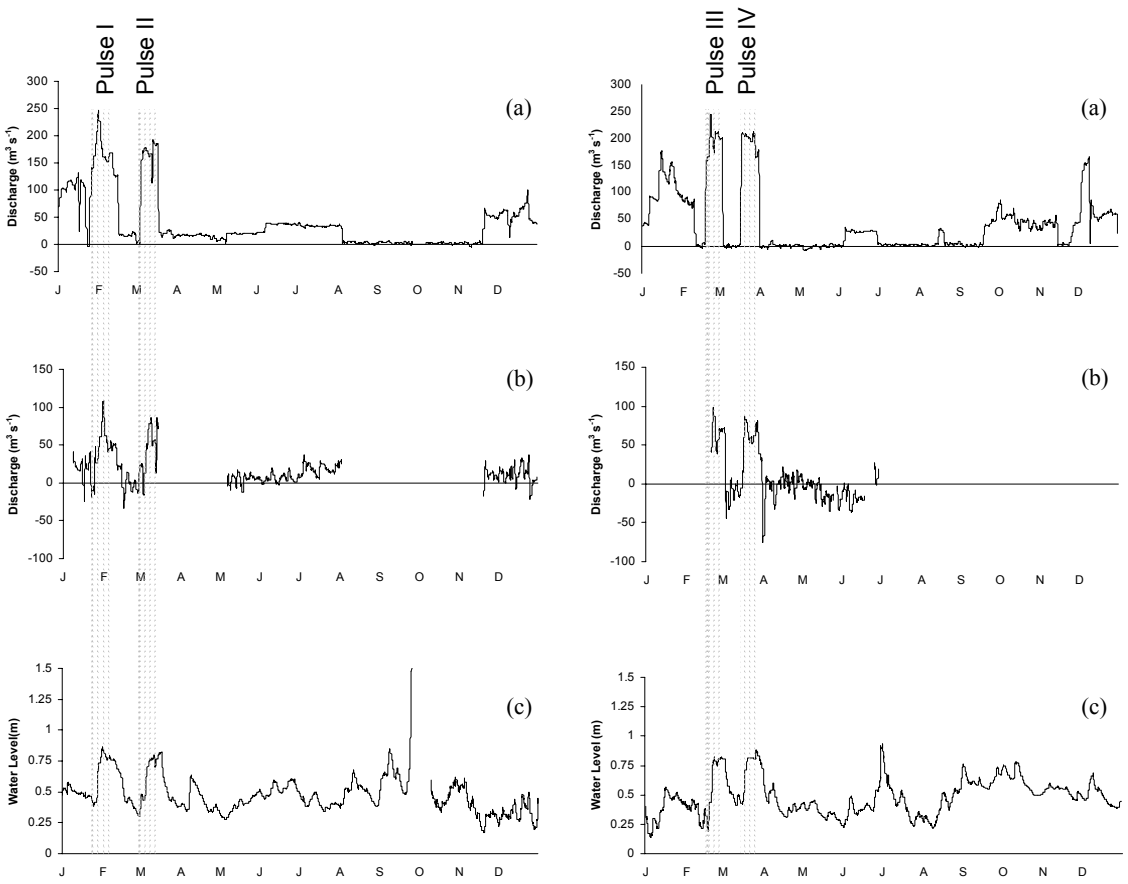

Figure 3.7. Time series of diversion discharge (a), residual discharge (b) and marsh water level (c) for 2002 (left) and 2003 (right). The shaded boxes indicate periods when pulsed diversions occurred. Gaps in the residual discharge time series indicate periods when data from one or more of the flow station was unavailable. The prominent spike in the water level time series during September 2002 reflects the passage of Tropical Storm Isadore.

discharge. Time periods when the diversion was closed, or when data from one or both of the downstream flow routes were unavailable were omitted. During the four pulsed diversions, the mean total discharge conveyed downestuary as channelized flow ranged from 107 m^3 s^{-1} to 122 m^3 s^{-1}. A sizeable residual discharge was associated with each event, indicating that marsh sheet flow tended to occur when a threshold discharge was exceeded at the head of the estuary. No significant sheet flow appeared to occur when fluvial inputs were less than 100 m^3 s^{-1}, as indicated by the lack of a substantial residual discharge during these times

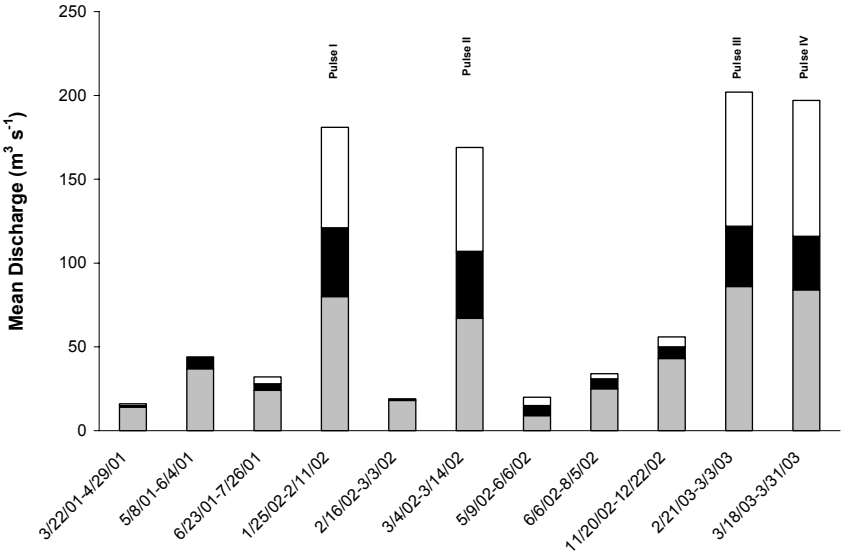

Figure 3.8. Mean distribution of discharge between the eastern (gray), western (black), and overland (residual; white) flow routes for various time periods. The total height of each bar indicates the mean diversion discharge for the given time period.

Discussion

River inputs at the head of the Breton Sound estuary during the course of this study were characterized by a pair of large, pulsed diversions in late winter to early spring, each lasting two weeks, followed by a period of very low to moderate inputs for several months, and then moderate to high inputs starting in December. Under these

conditions, annual sediment loading to the estuary was on the order of 1×10^5 metric tons yr^{-1}. Because the upper Breton Sound estuary is completely isolated from the Mississippi River by containment levees, the diversion structure is now the most important source of allochthonous mineral sediments for the marshes in this region.

Up to 51% of total annual sediment loading durng this study transpired during the four weeks when pulsed river diversions were occurring, suggesting that annual sediment delivery could be substantially augmented by increasing either their duration or frequency of occurrence. Diversion discharge is gravity-driven, and generally restricted to times of the year when river stage in New Orleans exceeds 1.2 m. Comparison of mean daily river stage in New Orleans, collected by the U.S. Army Corps of Engineers, with this threshold river stage (Figure 3.9) suggests that maximum capacity (225 $m^3 s^{-1}$) diversions are generally possible between Dec and Jul each year. Hence, assuming average TSS concentrations in the Mississippi River (Figure 3.2), potential river inputs to the estuary through the diversion could approach 4.5×10^5 metric tons yr^{-1}, nearly five times the annual inputs observed in this study. Such large, prolonged inputs of river water to the estuary are presently avoided because of a variety of anticipated adverse socioeconomic impacts, primarily reductions in commercial shellfish landings (Thomas 1999). The pulsed diversion events conducted in this study occurred between late winter and early spring, a time of year when these impacts tend to be minimal.

The results put forth here indicate that sediment inputs were maximized when diversion events coincided with flood pulses of the Mississippi River, particularly the rising limbs of such events. Pulsed diversions occurring under these circumstances delivered up to four times the quantity of sediment as those that occurred during troughs

in river discharge. The trends observed here are consistent with previous findings regarding temporal variability in Mississippi River TSS concentrations (Mossa 1986), where positive quadratic power relationships between river discharge and TSS were observed, with TSS peaks generally preceding discharge peaks. The lead time of the TSS peak relative to the discharge peak is highly variable, though, and while it is clear that fluvial inputs occurring during rising limbs of river floods enhanced sediment loading into the estuary, it is impossible to say if the loading was maximized due to the low temporal resolution of Mississippi River TSS data.

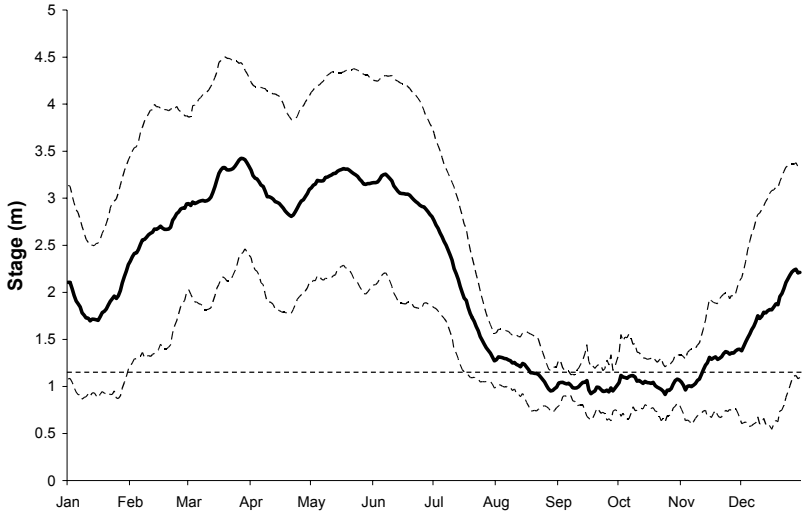

Figure 3.9. Average daily Mississippi River stage from 1993-2003 recorded at the Carrollton gauge in New Orleans, LA (thick line), with upper and lower standard deviations (dashed lines). The dotted horizontal indicates minimum river stage necessary for river diversions to occur.

This study illustrates the importance of high-discharge pulsed fluvial inputs not only in delivering large quantities of sediment to the Breton Sound estuary, but also in providing a transport mechanism for river sediments to reach the marsh interior regions where mineral deposition is needed to help offset RSLR. Comparison of discharge measured downestuary in the main eastern and western channels with discharge through

the diversion structure at the estuary head indicates periods when a large residual discharge exists. This residual flow is likely conveyed downestuary over the marsh as sheet flow in the upper estuary with a magnitude that is largely governed by the rate at which river water enters the estuary.

Interpretations of the residual discharge must be made with caution, however, as any measurement errors made at the three discharge stations will manifest themselves in the residual term. While present, these impacts should be negligible as the current meters used in this study were accurate to 1% of actual velocities. Because the current meters only measure velocity at one specific depth, rather than profile the entire water column, discharge estimates could also be sensitive to vertical positioning of the instruments. Despite this caveat on q_{resid}, flow in the oligohaline upper estuary is fully turbulent with a Reynolds number Re on the order of 1×10^7, calculated as

$$Re = \frac{UH}{\upsilon} \tag{3.4}$$

where typical velocities U in the outflow and east and west channels are near 1 m s^{-1} when river inputs are occurring, the characteristic depth H of the channel is on the order of 10 m, and the kinematic molecular viscosity υ of the introduced river water is taken as 1×10^{-6} m^2 s^{-1}. Thus, when river inputs are occurring, depth-dependent variability in current velocity in the upper Breton Sound estuary is likely minimal owing to turbulent mixing of momentum in the water column, and computations of discharge should be relatively insensitive to the vertical placement of the current meters within the water column.

Other notable sources that contribute to the freshwater budget in estuaries are precipitation and evapotranspiration. As such, the residual discharge may include water

fluxes not associated with the river diversion. In fact, precipitation was the primary freshwater source in the annual water budgets for the Breton Sound estuary from 2000 to 2002 (Hyfield et al. 2005). However, its relative importance varied throughout the year and during spring, when the pulsed river inputs were occurring, precipitation inputs became secondary to fluvial inputs through the diversion structure. Furthermore, net precipitation (precipitation-evaportranspiration) was small and groundwater inputs were negligible, suggesting that the residual flows observed during the pulse events primarily resulted from freshwater inputs via the river diversion.

Assuming wind effects are negligible, the system is capable of transporting river water downestuary as channelized flow at a rate near 100 $m^3 s^{-1}$. When diversion discharge exceeds this value, the remaining volume spills over bank and is conveyed as sheet flow, where velocities are slow enough for substantial deposition as the water is discharged across the marsh surface. These results imply that, for a given time-integrated volume of river water introduced to the estuary, pulsed inputs provide the greatest potential for deposition of mineral sediments over the subsiding interior marshes. As an example, while a 200 $m^3 s^{-1}$ diversion lasting 10 days and a 20 $m^3 s^{-1}$ diversion lasting 100 days may both load similar amounts of sediment into the estuary (assuming non-varying river conditions), shorter, higher discharge pulsed events result in sheet flow and sediment delivery to these regions.

In reality wind effects are not negligible, but are in fact quite pronounced during late winter/early spring, when cold fronts pass through every 4 to 7 days (Chuang and Wiseman 1983) and strongly influence shelf and estuarine currents and water levels. Using a two input linear systems model (Bendat and Piersol 1986), nearly 80% of water

level variability across periods of 5 to 20 days could be explained by river and meteorological forcing (Chapter 2), indicating effects from the two forcing functions are additive. Thus, setup prior to cold front passages may augment any marsh inundation already induced by the river diversion and cause more widespread flooding, increasing the spatial extent of the transport mechanism for sediments to reach the interior marsh regions. Diversions occurring after a frontal passage when water levels are sufficiently reduced, on the other hand, will inundate a much smaller region of the upper estuary, and may reduce the potential area available for deposition of sediments derived from Mississippi River inputs at the estuary head.

Relatively large amounts of fluvial sediments enter the Breton Sound estuary each year, but it is unclear whether the loading rates observed during this study facilitates marsh deposition rates that are sufficient to offset RSLR and reduce coastal land loss observed in the Breton Sound estuary. Using sediment traps, Wheelock (2003) showed that pulsed river inputs to the Breton Sound estuary significantly increased short term deposition rates in backmarsh areas, but only for sites located within 6 km of the diversion structure. Taking the impact region to be a semicircle extending 6 km from the diversion structure gives an area of 57 km^2. These findings are corroborated by the fact that water level is significantly coherent with diversion discharge at a site located 7 km from the diversion, but not at a site 30 km away (Chapter 2).

It is instructive to compare the sediment loading and depositional impacts of the pulsed inputs to the Breton Sound estuary investigated here with other diversions that have occurred along the lower Mississippi River (Table 3.3). Uncontrolled diversions, in the form of crevasse splays, were common products of seasonal flooding prior to the

Table 3.3. Sediment delivery and deposition for various diversions of the Mississippi River. Type indicates controlled (C) or uncontrolled (U). Values for deposition are based on spatially uniform deposition and assume 100% capture efficiency within the impact area. Units for delivery and deposition are expressed as per event (rows 1 to 5) and per year (rows 6 & 7). [1]Calculations based on mean of pulsed inputs from Table 2

	Date	Type	Area (km^2)	Sediment Delivery ($\times 10^6$ m^3)	Deposition (mm)	Source
Event						
1. Bonnet Carre historical	1849-1874	U	1675	61	26	Kesel 1989
2. Bonnet Carre pre-dam	1937-1950	C	1675	14	8.4	Kesel 1989
3. Bonnet Carre post-dam	1973-1983	C	1675	6	3.6	Kesel 1989
4. Caernarvon Crevasse	1927	U	226	20	89	Kemp (pers. communication)
5. Caernarvon Pulse[1]	2002-2003	C	57	0.02	0.3	this study
Annual						
6. Caernarvon Observed	2002-2003	C	57	0.07	1.3	this study
7. Caernarvon Maximum		C	57	0.32	5.6	this study

construction of containment levees along the river's banks. Crevasses provided a means for large, pulsed introductions of fluvial sediments to coastal marshes in the river's interdistributary receiving basins. The Bonnet Carre crevasse, located 30 km upstream from New Orleans, overflowed five times between 1849 and 1874 and delivered up to 61 $\times 10^6$ m^3 of sediment during each event assuming a sediment density of 1.4 metric tons m^{-3} (Kesel 1989). Spatially uniform deposition across an average impact area of 1675 km^2 for such an event would result in accretion rates of 26 mm $event^{-1}$. In the 1930s containment levees were placed along the Mississippi River and a water control structure was constructed to regulate discharge through the historical crevasse. Between 1937 and 1950 the structure was opened three times and delivered an average of 14 $\times 10^6$ m^3 of sediment during each event, which translates into a spatially-uniform deposition rate of 8.4 mm $event^{-1}$ (Kesel 1989; Table 3.3). Between 1973 and 1983, after extensive damming of the upper and middle reaches of the river and associated reductions in sediment loads (Kesel 1988), the structure was opened four times. Sediment delivery and deposition rates associated with each event were less than half those observed through the structure during the pre-dam (1937 to 1952) period (Kesel 1989; Table 3.3).

The present-day Caernarvon diversion structure at the head of the Breton Sound estuary also is situated where a previous uncontrolled Mississippi River flood occurred through a crevasse. Assuming the same sediment density as Kesel (1989) allows for comparison of sediment loading and deposition via controlled and uncontrolled river inputs at Caernarvon with those that occurred at Bonnet Carre (Table 3.3). A crevasse was created during a 500-year river flood event in 1927 when the east containment levee was dynamited in attempt to reduce rising stage and associated flooding threats to New

Orleans. Discharge through the crevasse at times exceeded 9000 $m^3 s^{-1}$, and as much as 28×10^6 metric tons of river sediments may have been delivered to the estuary and subsequently deposited as a 89 mm-thick layer across a 226 km^2 area (Table 3.3; Kemp unpublished data). Average sediment delivery occurring during the pulsed diversions at Caernarvon in 2002 and 2003 was 2.75×10^4 tons $event^{-1}$ (Table 3.2), which produced negligible deposition rates (Table 3.3) when compared to previous natural diversions of Mississippi River water.

Similar calculations can be made based on the annual sediment inputs to the estuary through the river diversion structure, which allow for comparison of the resulting deposition rates to the rate of RSLR. The annual delivery rates ($\sim 1 \times 10^5$ metric tons yr^{-1}) observed in this study distributed uniformly across the 57 km^2 impact area result in an average deposition rate of 1.3 mm yr^{-1} (Table 3.3), which is in good agreement with rates of recent deposition for the upper 3-10 cm of sediment cores determined by ^{210}Pb analysis (Wheelock 2003). Even if all fluvial inputs to the estuary are retained for deposition in the upper estuary (as assumed for these calculations) the present loading rates are inadequate to offset RSLR in the upper estuary, estimated to be 2.8 to 3.8 mm yr^{-1} through a combination of ESLR (1 to 2 mm yr^{-1}; IPCC 2001) and subsidence (1.8 mm yr^{-1}; Coastal Wetlands Planning, Protection, and Restoration Act 2002). Increasing the annual loading rate to 4.5×10^5 tons yr^{-1}, the maximum rate possible assuming average conditions for the Mississippi River, yields a deposition rate that exceeds the RSLR rate (Table 3.3).

While mineral sediment deposition is required for vertical accretion and marsh stabilization, organic matter accumulation as live root mass and peat plays a critical role

in vertical accretion in the Mississippi River deltaic plain. Mineral sediments also play an important role because they provide a source of nutrients for plant growth that ultimately results in organic matter accumulation (Nyman et al. 1990). Additionally, iron bound to clay particles can precipitate and neutralize sulfide toxins. Even in regions of the delta plain where mineral sediment via overland flow cause by diversions is not possible, diversions may still be beneficial in augmenting vertical accretion by reducing salinity and sulfide stresses on wetland plant communities in the receiving basin.

Conclusions

The results put forth here were obtained from the first intensive sediment loading study associated with any river diversion in coastal Louisiana. During both years of the study, annual sediment inputs were approximately 1×10^5 metric tons. Up to half of that delivery occurred during the two pulsed river input events during late winter to early spring, and nearly 90% of loading occurred during a four-month span when river discharge is typically greatest due to snowmelt and high precipitation in the upper midwestern United States. During an average water year for the Mississippi River, the potential exists to deliver nearly five times the sediment delivery observed in this study, if diversion discharge is maximized throughout the year. Because such aggressive operations are currently not feasible due to, among other things, conflicts with commercial fishing during autumn and late spring, the current pulsed diversion management plan could be optimized by timing the pulsing events to coincide with rising limbs of Mississippi River flood events in late winter and early spring.

When discharge of river water into the Breton Sound estuary was less than about 100 $m^3 s^{-1}$, fluvial inputs were confined to the main flow channels in the upper estuary.

Coinciding with large (>180 m^3 s^{-1}) pulses of river inputs were periods of elevated marsh water levels and large residuals in the upper estuary water budget, demonstrating that the pulsed events have the potential to induce sheet flow over the marsh surface. Thus, in addition to delivering large amounts of river sediments to upper estuary waterways, pulsed inputs can also serve to transport the fluvial materials to the subsiding wetlands in the upper receiving basin.

The Caernarvon diversion currently serves as the primary source of river (clastic) sediments to the Breton Sound estuary. Nevertheless, results of this study indicate current sediment loading rates are minor when compared to those resulting from previous controlled and uncontrolled diversions of the Mississippi River. Even when assuming 100% capture efficiency, the loading rates observed here are insufficient to offset present rates of RSLR.

Literature Cited

Barras, J.A., P.E. Bourgeois, and L.R. Handley. 1994. Land loss in coastal Louisiana 1956-90. National Biological Survey, National Wetlands Research Center Open File Report 94-01, 4 pp., 10 color plates.

Bendat, J.S. and A.G. Piersol. 1986. Random Data: Analysis and Measurement. Second Edition, Wiley, New York, 566 pp.

Carbognin, L., P. Teatini, P., and L. Tosi. 2004. Eustacy and land subsidence in the Venice Lagoon at the beginning of the new millennium. Journal of Marine Systems 51: 345-353.

Chuang, W.S. and W.J. Wiseman, Jr. 1983. Coastal sea level response to frontal passages on the Louisiana-Texas shelf. Journal of Geophysical Research 88: 2615-2620.

Coast 2050. 1998. Toward a sustainable Coastal Louisiana. Louisiana Coastal Wetland Conservation and Restoration Task Force (LCWRTF). Louisiana Department of Natural Resources, Coastal Restoration Division, Baton Rouge, LA.

Coastal Wetlands Planning and Protection Act. 2002. Geology of the Breton Sound Basin. WWW Page, www.lacoast.gov/geography/bs/index.asp

Coleman, J.M., H.H. Roberts, and G.W. Stone. 1998. The Mississippi River delta: an overview. Journal of Coastal Research 3: 698-716.

Day, J.W., Jr., D. Pont, P.F. Hensel, and C. Ibanez. 1995. Impacts of sea-level rise on deltas in the Gulf of Mexico and the Mediterranean: the importance of pulsing events to sustainablility. Estuaries 18: 636-647.

Hensel, P.F., J.W. Day, Jr., D. Pont, and J.N. Day. 1998. Short-term sedimentation dynamics in the Rhone River delta, France: the importance of riverine pulsing. Estuaries 21: 52-65.

Hyfield, E.C.G., J.W. Day, Jr., J.E. Cable, and D. Justic. 2005. Water and nutrient budgets in a Mississippi deltaic estuary receiving river re-introduction. Submitted to Biogeochemistry July 2005.

IPCC. 2001. Climate Change 2001: The Scientific Basis. Contribution of Working Group I to the Third Assessment Report of the Intergovernmental Panel on Climate Change [Houghton, J.T., Ding, Y., Griggs, D.J., Noguer, M., van der Linden, P.J., Dai, X., Maskell, K., Johnson, C.A. (eds.)]. Cambridge University Press, Cambridge, United Kingdom and New York, NY, USA, 881pp.

Junk, W.J., P.B. Bayley, and R.E. Sparks. 1989. The flood pulse concept in river-floodplain systems. Canadian Journal of Fisheries and Aquatic Sciences Special Publication 106: 111-127.

Kesel, R.H. 1988. The decline in the suspended load of the lower Mississippi River and its influence on adjacent wetlands. Environmental Geology and Water Science 11: 271-281.

Kesel, R.H. 1989. The roll of the Mississippi River in wetland loss in southeastern Louisiana, U.S.A. Environmental Geology and Water Science 13: 183-193.

McKee, K.L. and I.A. Mendelssohn. 1989. Response of a freshwater marsh plant community to increased salinity and increased water level. Aquatic Botany 34: 301-316.

Mendelssohn, I.A. and K.L. McKee. 1988. Spatina alternaflora die-back in Louisiana: time course investigation of soil waterlogging effects. Journal of Ecology 76: 509-521.

Morlock, S.E., N.T. Nguyen, and J.H. Ross. 2001. Feasibility of acoustic Doppler velocity meters for the production of discharge records from the U. S. Geological

Survey stream-flow-gaging stations: U. S. Geological Survey Water-Resources Investigations Report 01-4157, 56 pp.

Mossa, J. 1988. Discharge-sediment dynamics of the lower Mississippi River. Transactions of the Gulf Coast Association of Geological Societies 38: 303-314.

Mossa, J. 1996. Sediment dynamics in the lowermost Mississippi River. Engineering Geology 45: 457-479.

Nyman, J.A., R.D. DeLaune, and W.H. Patrick, Jr. 1990. Wetland soil formation in the rapidly subsiding Mississippi River deltaic plain: mineral and organic matter relationships. Estuarine, Coastal and Shelf Science 31: 37-52.

Reed, D.J. 1989. Patterns of sediment depositon in subsiding coastal salt marshes, Terrebonne Bay, Louisiana. Estuaries 12: 222-227.

Sestini, G. 1992. Implications of climatic changes for the Nile delta. In: Jeftic, L., J.D. Milliman, and G. Sestini (Eds.), Climatic Change and the Mediterranean. New York: Edward Arnold, pp. 535-601.

Stanley, D.J.. 1990. Recent subsidence and northeast tilting of the Nile delta, Egypt. Marine Geology 94: 147-154.

Thomas, R.G. 1999. Fish habitat and coastal restoration in Louisiana. American Fisheries Society Symposium 22: 240-251.

Turner, R.E. 1998. Wetland loss in the northern Gulf of Mexico: multiple working hypotheses. Estuaries 20: 1-13.

Wheelock, K.W., 2003. Pulsed river flooding effects on sediment deposition in Breton Sound Estuary, Louisiana. M.S. Thesis. Louisiana State Univ., Baton Rouge, Louisiana, USA.

Xiqing, C. 1998. Changjian (Yangtze) River Delta, China. Journal of Coastal Research 14: 838-858.

CHAPTER IV.

TEMPORAL AND VERTICAL VARIATIONS OF WATER FLOW BETWEEN BARATARIA BAY AND THE GULF OF MEXICO

Introduction

Bar-built estuaries are common features in deltaic landscapes throughout the world. Tidal constrictions are often key components of such landscapes, and water exchanges through these features can play an important role in governing the distribution and transport of particulate and dissolved nutrients throughout the estuary-shelf regime of deltaic ecosystems. These ecosystems serve as important nursery grounds for juvenile fish and shellfish, and recruitment of fish larvae as well as planktonic organisms into the estuary is largely dependent on such exchange processes. Shaw et al. (1985) suggested that estuarine recruitment of gulf menhaden (*Brevoortia patronus*) larvae advected westward along the Louisiana shelf by a westward coastal current is dependent upon individuals passing the mouth of the estuary during an inflow event. Dispersal of contaminants and pollutants can also be dictated by estuary-ocean exchange.

Interactions between wind stress, river discharge, and variations in tidal stirring power dictate the nature of estuary ocean exchange. It is now clear from numerous studies that wind stress can affect these exchanges in two distinct ways (Elliott and Wang 1978; Wang 1979; Wong 1990; Wong and Moses-Hall 1998; Janzen and Wong 2002). Wind stress can effect water exchange locally, where wind stress directly over the estuary transfers momentum from the atmosphere directly into the underlying water column producing vertically-sheared currents. As a remote effect, wind stress outside the estuary can induce setup or setdown in the coastal ocean, and these fluctuations then propagate into the estuary with associated barotropic currents. It is well known that river discharge

into an estuary, and the associated horizontal density gradient, can invoke baroclinic currents where seaward flow of relatively fresh water near the surface overlies landward flow of dense, saline water near the bottom (Pritchard 1955, Hansen and Rattray 1966). More recently, several studies have shown how the degree to which this gravitationally-induced circulation occurs can be modulated by spring-neap variations in tidal stirring power (Griffin and LeBlond 1990, Peters 1999, Masson and Cummins 2000).

This study utilized a 101-day time series record of current velocity collected with an upward-looking acoustic Doppler current profiler (ADCP) situated at the bottom of a tidal pass that connects the Barataria estuary, in southeast Louisiana, with the coastal ocean. The relative importance of tidal and subtidal exchanges was investigated, and the vertical structure of the subtidal flow field was examined. Variations in the vertical structure and magnitude of the flow field were then related to wind stress, tidal stirring power, and freshwater forcing.

Study Site

The Barataria estuary (Figure 4.1) is an interdistributary basin of the Mississippi River delta located immediately south and west of the Mississippi River in southeast Louisiana. The estuary's length axis is oriented toward 160ºT, and runs about 80 km from its head near Luling, Louisiana to its mouth, where communication with the Gulf of Mexico (GOM) primarily occurs through a series of five passes situated between barrier islands (Banas 1978). The upper estuary contains several large oligohaline lakes intermixed marshes, while hydrography in the lower estuary is dominated by two large tidal bays (Barataria and Caminada Bays) surrounded by saline marsh habitats. Though the system is bathymetrically complex, average depth in the estuary is generally around 2

m (Kjerfve 1973). Owing to its shallow depth and the wind energy available for mixing, the Barataria estuary is classified as a well-mixed system.

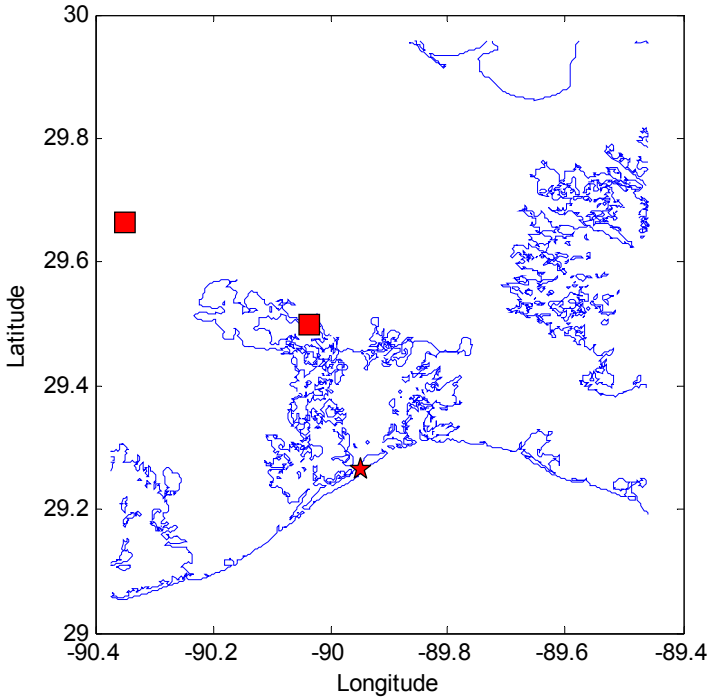

Figure 4.1. Map of the Barataria estuary. Wind speed and direction and current velocity data were obtained from Barataria Pass (star). Salinity was measured in the Gulf Intracoastal Water Way and at Little Lake (squares).

Freshwater inputs to the estuary primarily occur through a combination of several factors. Precipitation is on the order of 160 cm yr^{-1} (Byrne et al 1976). Surface runoff enters the estuary through several streams, most notably Bayou Des Allemands, and averages around 150 m^3 s^{-1} (Park 2002). Three Mississippi River diversion structures discharge into the Barataria estuary. The Davis Pond diversion, located at the head of the estuary, averaged approximately 5 m^3 s^{-1} during the study. Two other smaller diversions, West Point a la Hache and Naomi, are located further downestuary, and discharge through these structures averaged 33 and 22 m^3 s^{-1}, respectively. Finally, the Atchafalaya River discharges freshwater into the estuary, through a connection with the Gulf

Intracoastal Waterway (GIWW) at an average rate of 50 m^3 s^{-1} (Park 2002) , though this rate can be much greater when the river is in flood (Swarzenski 2003).

Exchange between the bays at the seaward end of the estuary and the Gulf of Mexico (GOM) primarily occurs through a series of five passes, Barataria Pass, Caminada Pass, Pass Abel, Quatre Bayou Pass, and Grand Bayou Pass, each situated between barrier islands. Nearly half the water exchange through these inlets occurs in Barataria Pass, which is relatively deep and wide ($h \approx 12$ m; $w \approx 1$ km); the remaining flux is distributed relatively evenly between the four other primary inlets (U.S. Geological Survey, unpublished data).

Sea level variability over the southeastern Louisiana continental shelf occurs over a broad range of time scales. Astronomical tidal amplitudes are weak and diurnal, with only the O_1 and K_1 constituents exceeding 5 cm. Over timescales of a few days wind stress becomes important in governing shelf sea levels, particularly during autumn and winter when the passage of winter storm systems occurs every 4-7 days (Chaung and Wiseman 1983) and cause shelf sea levels to fluctuate with typical amplitudes of 0.5 m.

Methods

Current meter measurements, provided by the Louisiana Department of Natural Resources, were made between 20 Dec 2002 and 3 Apr 2003 in Barataria Pass with a 1200 kHz RD Instrument Workhorse Sentinel acoustic Doppler current profiler (ADCP). The vertical resolution of the ADCP was set to 1 m and current speed and direction were recorded as 5-minute averages of 2 Hz bursts sampled every 15 minutes. Wind velocity, measured every hour at Grand Isle by the U.S. Coast Guard, was used to estimate wind stress following Large and Pond (1981).

To examine the subtidal current variability in Barataria Pass, cross-wavelet analysis (Torrence and Webster, 1999; Grinsted et al. 2004) was performed on low-pass filtered current velocity and wind stress data. The filter used was a Lanczos cosine filter with a half-amplitude period of 40 h (Emery and Thompson 2001). The wavelet transform is effective in analyzing time series that contain nonstationary energy at multiple frequencies (Torrence and Campo 1998). A wavelet is a function with zero mean that is localized in both time and frequency. One particular wavelet, the Morlet, is defined as

$$\psi_o(\eta) = \pi^{-1/4} e^{i\omega_o \eta} e^{-\frac{1}{2}\eta^2} \quad \textbf{(4.1)}$$

where ω_o is dimensionless frequency and η is dimensionless time A Morlet wavelet is used here because it provides a good balance between time and frequency resolution. A set of scaled and translated versions of ψ_o,

$$\psi_{\tau,s} = \frac{1}{\sqrt{s}} \psi_o \left(\frac{t-\tau}{s} \right) \quad \textbf{(4.2)}$$

can be obtained, where translation parameter τ corresponds to time and scale parameter s corresponds to scale length or temporal period. In a Morlet wavelet with $\omega_o = 6$ there are roughly three oscillations in the wavelet envelope, and frequency = 1.03s, making the wavelet scale nearly equal to the Fourier period, and essentially allowing the terms to be used interchangeably. The wavelet transform W_x of the time series x can then be acquired through the convolution of x with $\psi_{\tau,s}$:

$$W_x(\tau, s) = \sum_{n=0}^{N-1} x \cdot \psi^*_{\tau,s} \quad \textbf{(4.3)}$$

where * denotes complex conjugate. Thus, equation (4.3) expands the one dimensional time series into a two-dimensional space (τ, s) which corresponds to the time-frequency

domain, and provides a localized measure of the relative energy at scale s at time τ. This procedure differs from the traditional Fourier transform that yields an amplitude at scale s time-averaged over the entire dataset. Thus, wavelet analysis is quite useful for identifying periodic signals in nonstationary data. Wavelet power is defined as $\left|W_x(\tau,s)\right|^2$.

Given two time series x and y, with wavelet transforms $W_x(\tau, s)$ and $W_y(\tau, s)$, the cross-wavelet transform is defined as

$$W_{xy}(\tau,s) = W_x(\tau,s)W_y(\tau,s)* \tag{4.4}$$

and the cross-wavelet power is $\left|W_{xy}(\tau,s)\right|^2$. Cross-wavelet power indicates regions in time-frequency space with high common power. Another useful measure, wavelet coherence, indicates the localized correlation between two time series in time-frequency space, and is estimated as

$$R^2(\tau,s) = \frac{\left|\left\langle s^{-1}W_{xy}(\tau,s)\right\rangle\right|^2}{\left\langle s^{-1}\left|W_x(\tau,s)\right|^2\right\rangle\left\langle s^{-1}\left|W_y(\tau,s)\right|^2\right\rangle} \tag{4.5}$$

where $\langle\ \rangle$ indicates smoothing in both time and scale. Finally, the wavelet-coherency phase spectrum is estimated as

$$\phi_{xy}(\tau,s) = \tan^{-1}\left(\frac{\mathrm{Im}\left\{\left\langle s^{-1}W_{xy}(\tau,s)\right\rangle\right\}}{\mathrm{Re}\left\{\left\langle s^{-1}W_{xy}(\tau,s)\right\rangle\right\}}\right) \tag{4.6}$$

Smoothing in (4.5) and (4.6) was performed according to Torrence and Webster (1999), where the wavelet matrix is convoluted with a weighted running average window in both the time and frequency dimensions. Smoothing in time is done with a Gaussian window

identical to the absolute value of the wavelet transform at each scale, normalized to have a total weight of unity. Smoothing in scale is done with a boxcar filter having a width of 0.6, the scale-decorrelation length for the Morlet wavelet function. Statistical significance levels of wavelet coherence were estimated using Monte Carlo methods following Grinsted et al. (2004).

Results

Tidal Variability

Principal axis analysis (Emery and Thompson 2001) of unfiltered hourly current velocity showed the data to be largely rectilinear, with the major axis exceeding the minor axis by more than an order of magnitude. The orientation of the current variance major axis corresponded well with the axis of Barataria Pass (Figure 4.2). With the exception of a slight decrease in velocity near the bottom, likely due to bottom friction (Fig 4.3), the vertical structure of the unfiltered velocity along the major axis of the flow field was largely depth-independent. Thus, further analysis of tidal timescale variability was conducted on the depth-averaged velocity component along the major axis, where positive values indicate seaward (ebb) flows through the pass. Visual inspection of the unfiltered hourly data shows a clear dominance of the tidal signal in the total variability of the current time series.

Estimates of tidal constituent amplitude and phase for flows through the pass were obtained by least-squares harmonic analysis (Dronkers 1964; Table 4.1). A total of 35 constituents were extracted, and tidal fluctuations accounted for greater than 84% of total current variability in Barataria Pass. Over 80% of the total current variance could be explained by a combination of the O_1 and K_1 constituents. Contributions by semi-diurnal

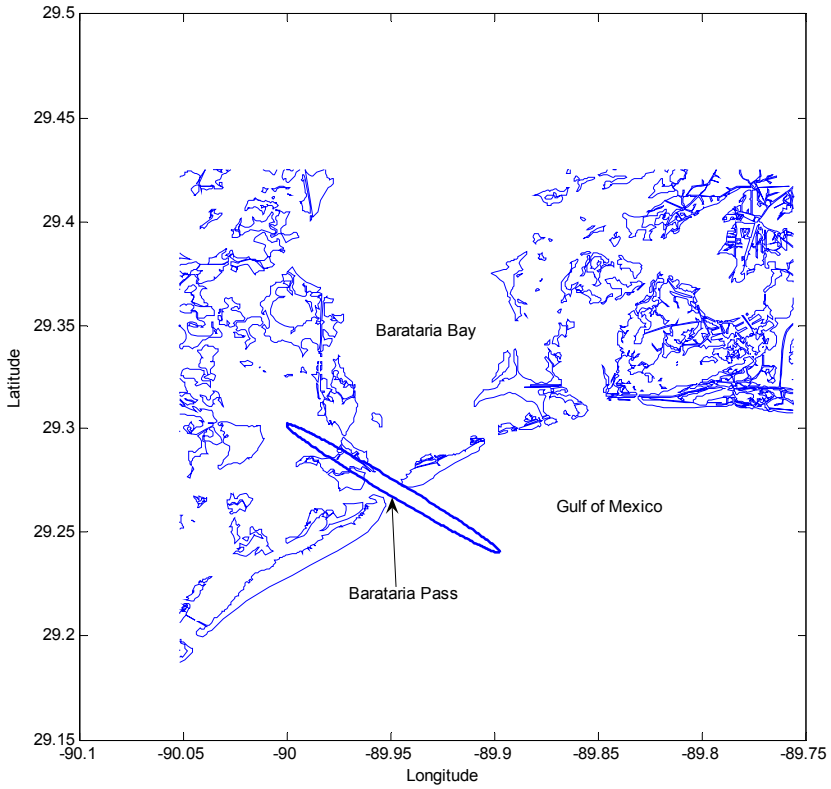

Figure 4.2. Orientation of unfiltered depth-averaged current velocity ellipse in Barataria Pass.

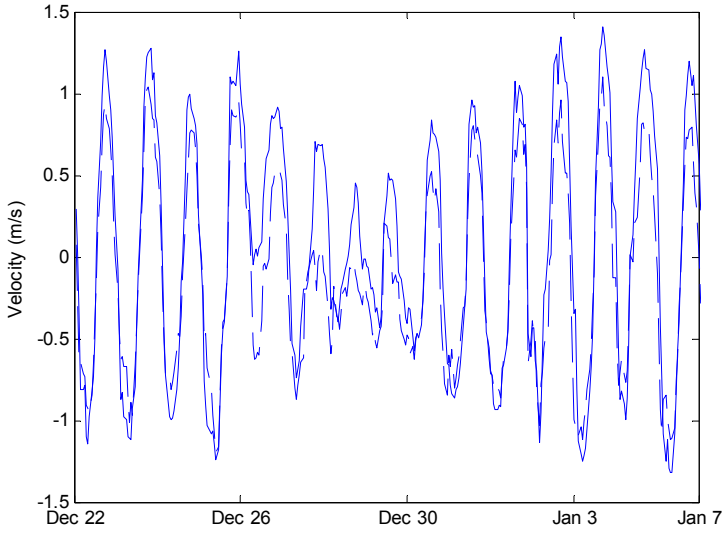

Figure 4.3. Time series of the axial component of near-surface and near-bottom unfiltered current velocity in Barataria Pass between Dec 22 and Jan 7.

Table 4.1. Tidal constituent percent total current variance, amplitude, phase, and excursion distance over half of a tidal cycle for four major constituents in Barataria Pass.

Constituent	Period (h)	% Variance	Amplitude ($m\ s^{-1}$)	Phase (degrees)	Tidal Excurison (km)
O1	25.81	37.0	0.52	205	15.6
K1	23.93	44.4	0.57	284	15.4
M2	12.42	0.3	0.05	107	0.8
S2	12.00	0.1	0.02	255	0.5

constituents were negligible, with the variance contribution of the S_2, M_2, and N_2 constituents being less than 1%. The tidal form number, calculated as the ratio of the main diurnal to semidiurnal component amplitudes, $(K_1 + O_1)/(M_2 + S_2)$, was 12.75, indicating that tidal currents in the pass were almost entirely diurnal.

Tidal excursion over half of a tidal cycle can be computed as UT / π, where U is the amplitude of the tidal current constituent in km hr^{-1} and T is the period of the constituent in hours. These calculations are useful for determining the relative importance of the tidal constituents in exchanging water between Barataria Bay and the Gulf of Mexico through Barataria Pass. Again, the diurnal components were clearly dominant in this regard (Table 4.1). Under tropical tides, when the K_1 and O_1 constituents are in phase and they constructively interfere (i.e., they are additive), total diurnal excursions exceeded 31 km. On the other hand, during equatorial tides when the two diurnal constituents destructively interfere, diurnal tidal excursions were less than 0.5 km.. Excursions for the M_2 and S_2 constituents were 0.75 km and 0.45 km, respectively (Table 4.1).

Subtidal Variability

The top panel of Figure 4.4 shows near surface and near bottom subtidal current velocities in the pass. Subtidal currents were usually under 0.5 m s^{-1}, and though fluctuations appeared to be largely depth-independent, there were several brief episodes where considerable current shear was evident. The lower panel of Figure 4.4 shows wind stress during the study. Winds were generally blowing southward during the study, and the passage of several winter frontal systems is evident, particularly during the first 50 days of the study. Wind stress was notably less during the second half of the study period.

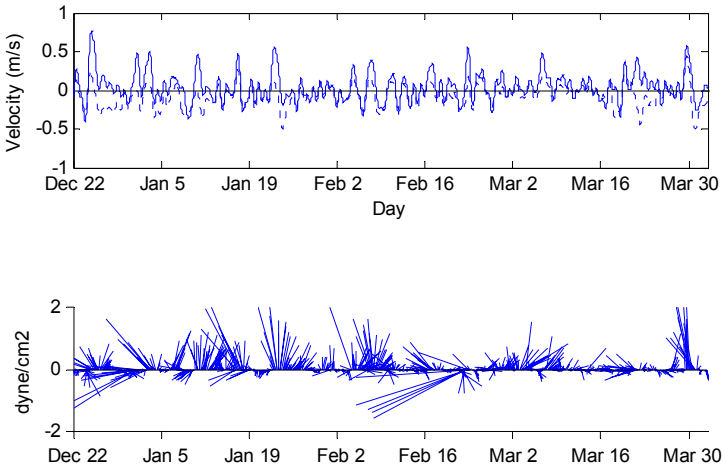

Figure 4.4. Time series of subtidal current velocities through Barataria Pass (upper panel; solid line represents near surface currents, dashed line represents near bottom currents). Vector plot of wind stress (lower panel). A vector extending upwards from the x-axis indicates wind blowing from the north. Vector length indicates magnitude of wind stress.

A minor flood event was occurring on the Atchafalaya River during the onset of the study in late Dec (Figure 4.5). River stage crested near bankfull stage (+1.2 m NAVD 88) on Jan 2, after which it gradually declined to a minimum of 0.25 m on Feb 8. The river stage then gradually increased again, exceeding bankfull stage on Feb 28 and

peaking again on Mar 17 at 1.6 m. A corresponding inverse pattern in salinity in the GIWW, which connects the lower Atchafalaya River to the estuary, and in the estuary itself at Little Lake was evident. A correlation coefficient of -0.63 between Atchafalaya River discharge and Little Lake salinities was present, where salinity lagged river discharge by 9 days (Figure 4.6).

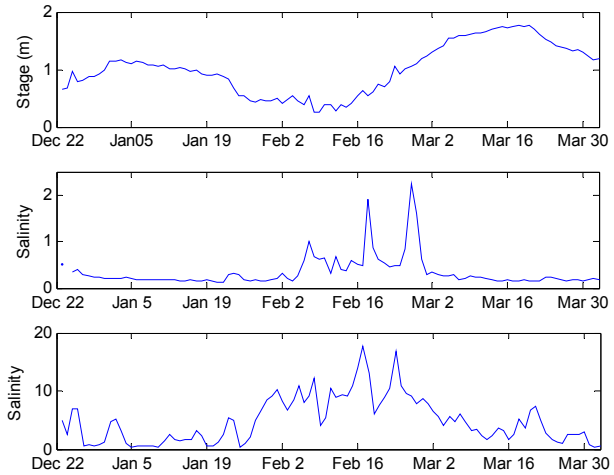

Figure 4.5. Time series of Atchafalaya River stage (upper panel), salinity in the GIWW (middle panel) and salinity in the estuary at Little Lake (lower panel) during the 101-day data collection period.

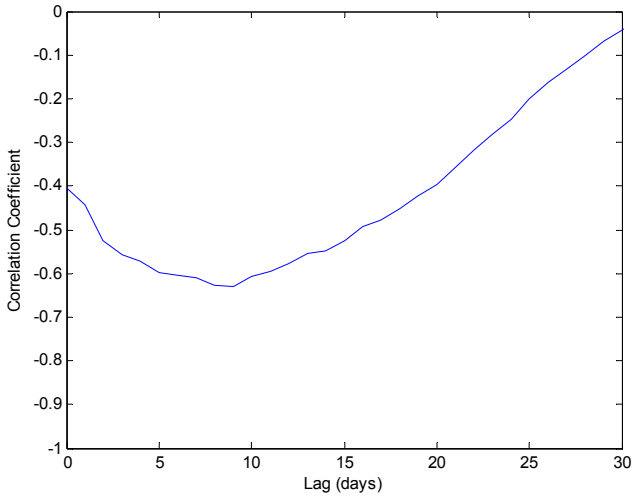

Figure 4.6. Correlation coefficients between Atchafalaya River stage and estuarine salinity recorded at Little Lake. Maximum correlation occurred when salinity lagged river stage by 9 days (r = -0.63).

The wavelet spectra for alongshore and cross-shelf wind stress are presented in two ways in Fig 4.7. The wavelet power spectrum is shown in the upper left. To the right is the global wavelet spectrum, calculated as the time average of wavelet power as a function of frequency (analogous to a Fourier spectrum). The along-shelf wind stress showed energy peaks between across 2-4 d periods in late Dec and another peak in late Feb. Aside from these episodes there was relatively little energy in the alongshore wind stress. The cross-shore wind stress variability was relatively uniform in its distribution across both time and frequency space, with regions of higher energy associated with periods of 3-10 days. This periodicity is consistent with the typical recurrence interval of frontal passages in the northern GOM (Angelovich, 1976). The energy of the cross-shelf wind field is demonstrably less in the second half of the study period.

Empirical orthogonal function (EOF) analysis (Preisendorfer 1988) was performed on the ADCP data set to provide a description of the dominant modes of vertical variation of currents in Barataria Pass. EOF analysis optimally partitions the variance of a field into orthogonal spatial patterns (modes) that are simply the eigenvectors of the data field's covariance matrix. Each mode has a corresponding eigenvalue that is proportional to the percentage of the total variance each mode accounts for. Each mode is also associated with a time series (principal component; PC) that describes its evolution through time. EOF solutions were normalized to their standard deviations, giving each principal component a variance of unity and, thus, amplitudes on each eigenvector carries units in m s^{-1}.

The first two modes accounted for 99.6% of the total subtidal flow variability in Barataria Pass. Over 90% of the total variability could be attributed to mode 1, which

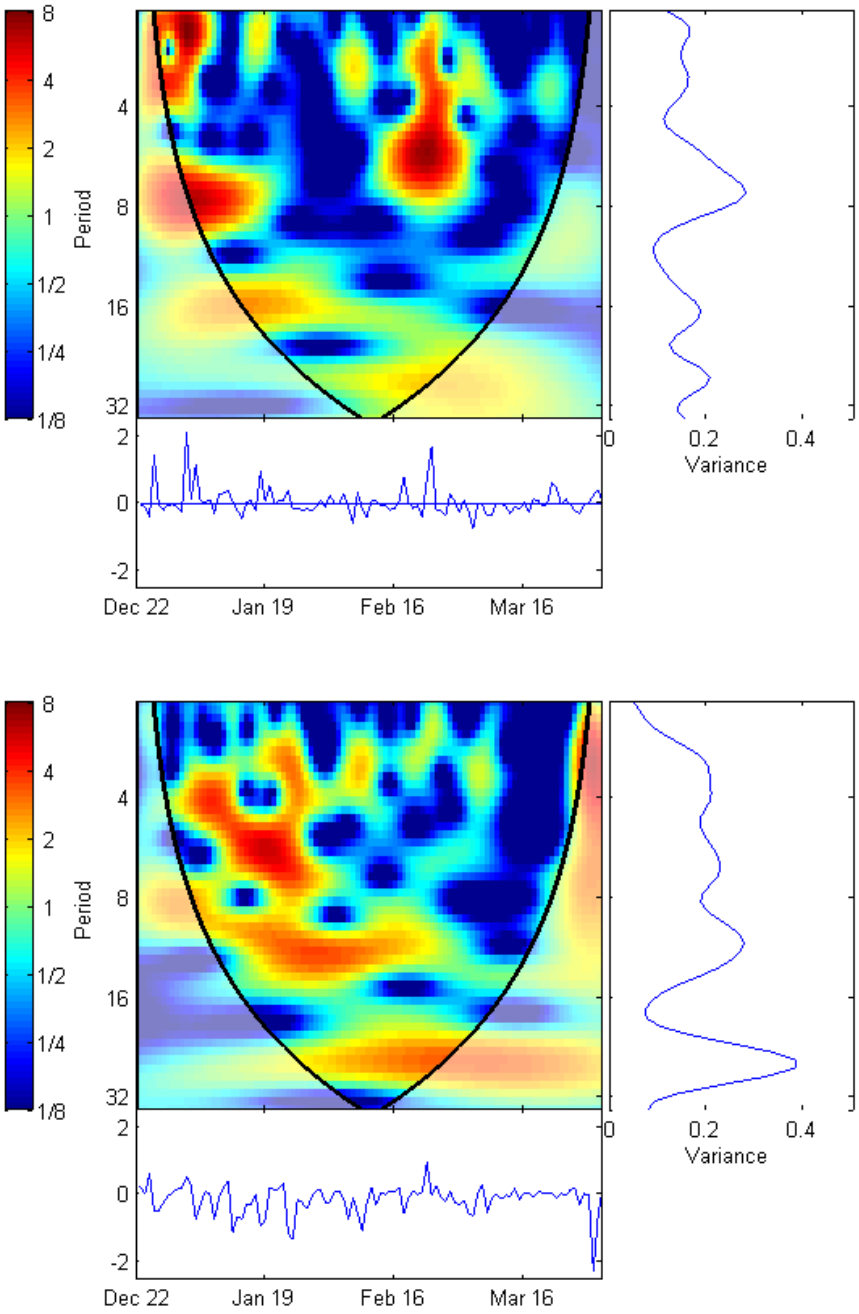

Figure 4.7. Wavelet power spectra for alongshore (upper) and cross-shelf (lower) wind stress. In each plot, the time-evolution of wavelet power, normalized to the time series variance, is shown by the contour plot. To the right is the global wavelet spectrum. On the bottom is the time series of the wind stress data.

carries the same sign throughout the water column, with a slight magnitude decrease with increasing depth (Figure 4.8). Hence, mode 1 describes unidirectional flow, from surface

to bottom, of water in or out of the estuary, and serves as a metric of barotropic exchanges that occurred between Barataria Bay and the continental shelf. The second mode accounted for slightly greater than 8% of the total flow field varibility. Unlike the first mode, a reversal in sign at roughly mid-depth exists, and this mode hence represents exchanges through the pass where the surface currents opposed those at the bottom (Figure 4.7). Thus, mode 2 describes a vertically sheared flow through the pass. None of the remaining 12 modes comprise greater than 0.2% of the total flow variability.

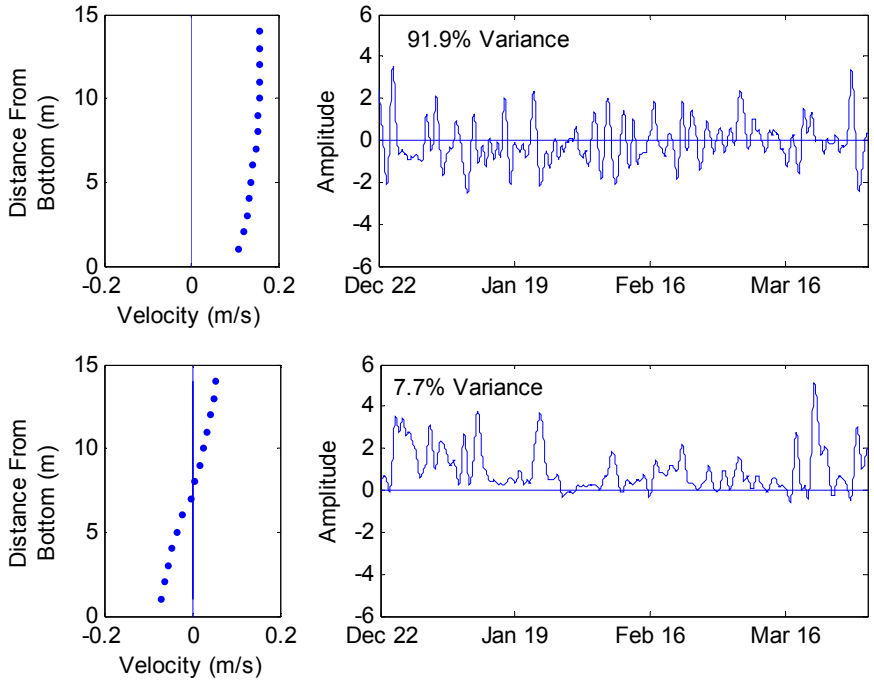

Figure 4.8. Vertical distributions of EOF eigenvector amplitudes (left) and principal component time series (right) for EOF modes 1 (upper) and 2 (lower). The EOF solutions have been normalized so that the eigenvector amplitudes have units of m s^{-1} and the principal component time series have a non-dimensional variance of unity.

Positive (negative) values for the time series describing the temporal evolution of the EOF mode 1 response (PC1) indicate outflows (inflows) through the pass. A pronounced energy peak near 3-day periods exists in the global wavelet spectrum (Figure 4.9). Consistent with the cross-shelf wind stress, the wavelet power spectrum of PC1

shows the variability in the 3-day band subsided during the second half of the study period.

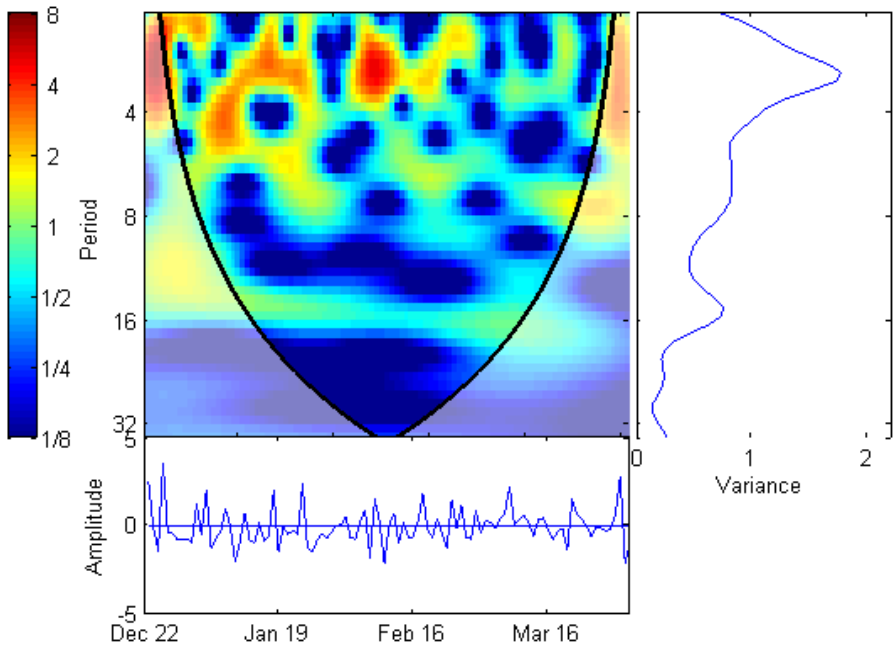

Figure 4.9. Wavelet power spectrum, global wavelet spectrum, and time series for EOF mode 1.

Cross-wavelet analysis was used to investigate the influence that cross-shelf and alongshore wind stress exerted on barotropic exchanges in the pass (Figure 4.10). Brief occurrences of significant coherence existed between the alongshore winds and PC1 across periods of 2-4 days, but these events were ephemeral. Phase in these coherent regions of time-frequency space was near zero, consistent with Ekman divergence at the coast facilitating barotropic outflows through the pass; a positive (east) alongshore wind was associated with a positive (outflow) current through the pass. The region of time-frequency space where significant coherence existed between cross-shelf winds and PC1 was much larger. This region spanned periods of 3-8 days and was persistent throughout

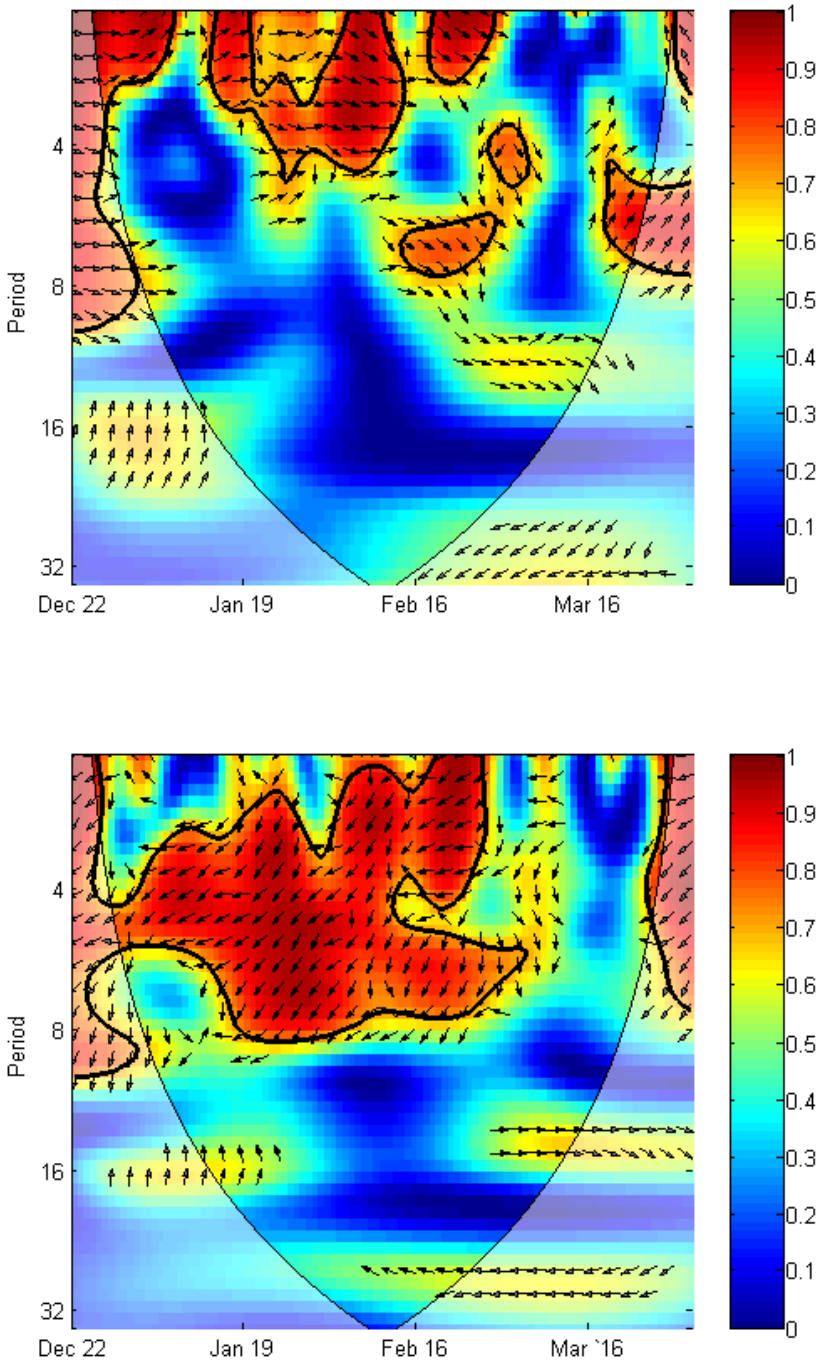

Figure 4.10. Wavelet coherence and phase between east-west (upper) and north-south (lower) wind stress components with time series for EOF mode 1. Solid lines delineate regions of time-frequency space where coherence between the time series is significant at $\alpha = 0.05$. Phase is indicated by the direction of the arrows, where an arrow pointing toward the right indicates an in-phase relationship, an arrow pointing downward indicates the second variable lags the first by 90º, a leftward-pointing arrow indicates the two variables are out of phase 180º, and an upward pointing arrow indicates the second variable leads the first by 90º.

most of the study period; the exception being a brief period in mid-March when, coincidentally, wavelet power for cross-shelf wind was quite low (Figure 7). The phase relationship between cross-shelf wind and PC1 was generally between -90º and -180º, indicating that a negative (inflow) current through the pass lagged a positive (northward) cross-shelf wind stress.

To obtain increased directional resolution with regard to which wind stress directional component was most effective at forcing EOF mode 1 current fluctuations through the pass, coherence analysis (Bendat and Piersol 1986) was performed between PC1 and each directional component of wind stress between -90ºT and 90ºT at 5º increments (Figure 4.11). A band of high coherence (> 0.7) centered about a predominantly cross-shelf direction existed for all frequencies greater than about 0.15 cpd. The direction of maximum wind forcing θ as a function of frequency can be estimated by

$$\theta = \frac{\pi}{2} + 0.5 \tan^{-1} \frac{2|h_1||h_2|\cos\phi}{|h_1|^2 - |h_2|^2} \qquad \textbf{(4.7)}$$

where h_1 and h_2 are partial transfer functions relating orthogonal wind stress components, in this case cross-shelf and alongshore wind stress components, to current velocity and φ is the phase difference between h_1 and h_2 (Garret and Toulany 1982). Between periods of 2 and 8 days, timescales where coherence between wind stress and PC1 was significant, the mean direction of maximum wind stress forcing was largely along a cross-shelf axis (-20ºT). The phase between the wind stress component along -20ºT (not shown) was near 135º across these timescales, indicating that mode 1 inflows through the pass lagged onshore winds by about 45º. Coherence of PC1 with winds oriented with the alongshore axis was minimal. These results are in good agreement with the results of cross-wavelet

analysis between mode 1 flows through the pass and the pair of orthogonal wind stress components.

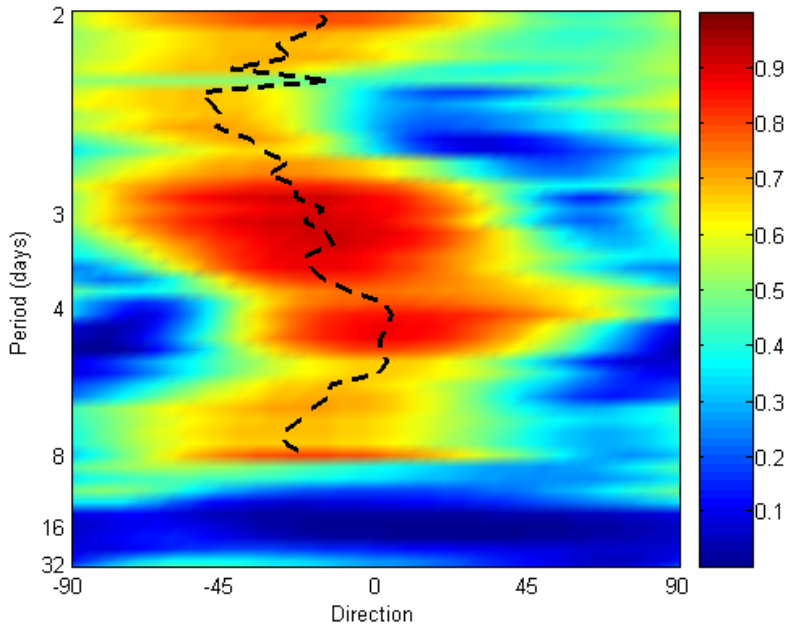

Figure 4.11. Coherence squared between η_o and wind stress components along the directions of -90º T – 90º T in 5º increments, obtained from spectral analysis. The dashed line indicates the direction of maximum wind forcing, estimated according to Garrett and Toulany (1982).

The time series describing the temporal pattern of the sheared flow response (PC2) nearly always carries a positive sign (Figure 4.8). Thus, flows associated with EOF mode 2 can be characterized by outflow in the upper water column and inflows near the bottom, and resemble what one might expect from traditional baroclinic estuarine circulation theory. The global wavelet spectrum showed a pronounced energy peak at 14-day periods, and the wavelet power spectrum demonstrated this feature to be persistent throughout the study period, though it did weaken considerably in late-Feb to early-Mar (Figure 4.12).

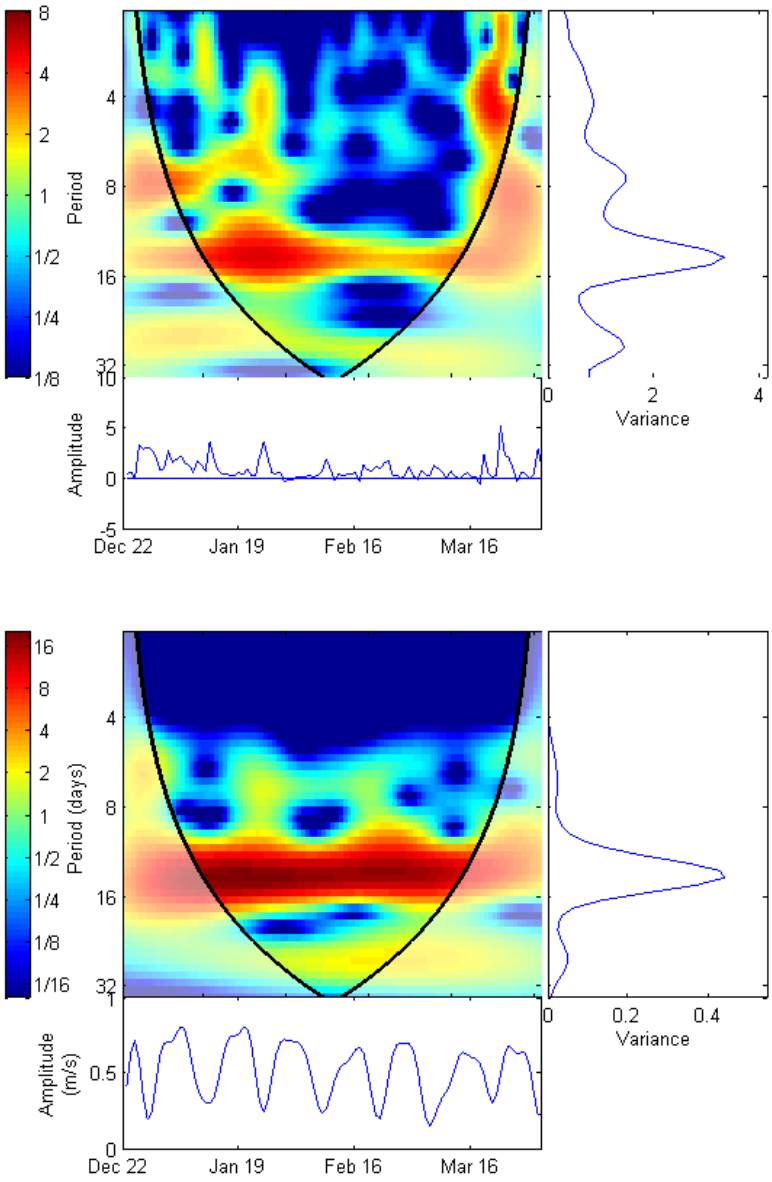

Figure 4.12. Wavelet power spectrum, global wavelet spectrum, and time series for EOF mode 2 (upper) and complex-demodulated diurnal tidal current amplitude (lower).

To investigate the role that fortnightly variations in the diurnal tidal amplitude associated with interactions between the K_1 and O_1 tidal constituents may have played in regulating episodes of vertically-sheared flow in Barataria Pass, complex demodulated tidal current amplitude through the pass was compared with PC2. Complex demodulation (Bloomfield 1976) estimates the time evolution of the amplitude of a time

series at a specified frequency f_o. Here the diurnal tidal frequency is to be enveloped, so f_o is taken as 0.0403 cpd, which is the center of a frequency band that spans the frequencies of the O_1 and K_1 constituents. Multiplication of the current velocity time series by a complex exponential of frequency f_o gives

$$U_d(t, f_o) = u(t)e^{-i2\pi f_o t} \quad \textbf{(4.8)}$$

This procedure frequency shifts the data so that all frequencies f of $U_d(t, f_o)$ are now $f - f_o$ and hence f_o now has a frequency of zero. The frequency-shifted time series is then smoothed with a low-pass filter to eliminate higher-frequency fluctuations not associated with f_o. Here, a low-pass Lanczos filter with a half-amplitude cutoff period of 120 hours was used. Variability in the resulting complex time series $U_d(t, f_o)$ in a band near the central frequency can be expressed in terms of a time-varying amplitude $\left|U_d(t, f_o)\right|$.

The time series of tidal current amplitude, along with its wavelet spectra, are shown in Figure 4.12. The amplitude of the diurnal tidal currents ranged between about 0.1 and 0.8 m s^{-1}, and the oscillations of the signal showed a clear fortnightly cycle. Wavelet coherence between tidal current amplitude and PC2 showed that fortnightly variations in the two time series was highly coherent (Figure 4.13). Furthermore, they vary out of phase by nearly 180º, which indicates that the presence of vertically sheared flow in the pass tended to occur coincidentally with periods of low tidal current amplitude.

Discussion

The ADCP data indicated that tidally-induced flow was responsible for 85% of the total current variance in Barataria Pass, and that nearly all the tidal forcing resulted

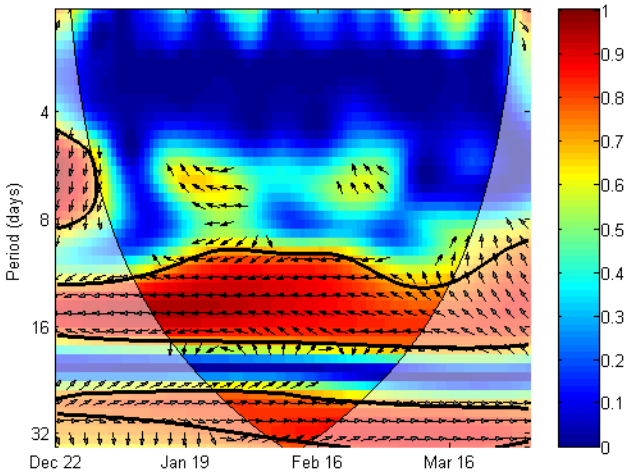

Figure 4.13. Wavelet coherence and phase between complex-demodulated diurnal tidal current amplitude and time series for EOF mode 2.

from roughly equal contributions of the O_1 and K_1 constituents. Tidal excursions can be interpreted in the context of the geometry of the pass. Excursions of roughly 30 km during tropical tides were clearly sufficient to facilitate materials exchange between Barataria Bay and the adjacent shelf. On the other hand, during equatorial tides the excursions were an order of magnitude less than the length of the pass, suggesting that other forms of transport, such as meteorologically- or gravitationally-induced exchanges, may have become more important.

EOF analysis was effective in decomposing the vertical structure of the subtidal current velocity data into two dominant modes of variability that accounted for greater than 99% of the total variance. The flow was predominantly barotropic, and bottom friction was evident this mode, as indicated by the amplitude reduction in the mode 1 eigenvector near the bottom of the water column. It is well-documented that the alongshore wind plays a key role in facilitating barotropic estuary-shelf exchange through the induction of sea level slopes at the estuary-shelf interface by Ekman convergence/divergence. Yet this dynamic appeared to be relatively unimportant in

effecting barotropic exchanges through Barataria Pass, as shown by the results of the wavelet coherence analysis between the alongshore wind stress and PC1. Instead, coherence between the cross-shelf component of wind stress and PC1 existed over a broad domain of time-frequency space, and phase between the two time series suggests that winds blowing toward the coast forced barotropic inflows of shelf waters into the bay. Wong (2002) found that subtidal currents in Indian River Inlet, DE, responded to two distinct wind stress directional components, one widely distributed along the alongshelf direction and another relatively narrow band situated about the cross-shelf axis. The first case resulted from Ekman setup/setdown at the coast, and the second from direct setup forced by onshore/offshore winds over the shallow inner shelf.

The dominance of cross-shelf wind stress in forcing barotropic exchange through the pass may be a result of sea surface slope induction across Barataria Bay brought about by local atmospheric forcing. Northward wind stress acting over the bay may result in setup at the northern end of the bay, with coincident setdown at the southern end. Thus, sea levels immediately inside the pass would be lower than those outside on the continental shelf, and a pressure gradient that favored barotropic inflows through the pass would result. The reverse would occur during southward winds: sea levels would setup at the southern end of the bay, causing a pressure gradient that favored depth-independent outflows through the pass.

The second mode extracted from the EOF analysis was characterized by strong vertical shear and the pattern is consistent with gravitationally-driven estuarine circulation in the sense that flow in the upper portion of the water column was overwhelmingly seaward while flow in the lower portion was directed landward. No

substantial reversals in this pattern occurred during the 101-day study. Results of cross-wavelet analysis indicate that there was strong coupling between the diurnal tidal current amplitude and PC2 across fortnightly timescales, and that the velocity shear was greatest during periods when the tidal current amplitude was low (equatorial tides). On the west coast of North America, freshwater outflows in Juan de Fuqua Strait were found to be enhanced during spring tides, owing to decreased tidal mixing (Griffin and LeBlond 1990). In Bertioga Channel, Brazil, upstream salt transport driven by gravitational circulation was observed to exceed that of tidal salt flux by a factor of 2.6 during neap tides, while during spring tides the tidal flux term exceeded the gravitational term by a factor of 1.4 (de Miranda et al 1998). A momentum balance of currents measured at the mouth of Chesapeake Bay revealed fortnightly amplification of the baroclinic term that occurred during neap tides (Valle-Levinson 1995).

Tidal mixing power is determined by the parameter u^3/h (Simpson and Hunter 1974). When that parameter exceeds a critical value, stratification, and thus baroclinicity, is diminished due to turbulence. Tidal current amplitudes in Barataria Pass ranged from around 0.2 m s^{-1} during equatorial tides to about 0.8 m s^{-1} during tropical tides, indicating that tidal mixing power varied by over a factor of 60 during the tropical-equatorial cycle. Though density profiles were unavailable to measure any ensuing influences on stratification in Barataria Pass, Peters (1997) observed that changes in tidal current amplitude from 0.85 m s^{-1} to 1.12 m s^{-1} over the spring-neap cycle near the mouth of the Hudson River, New York, resulted in reductions in surface-to-bottom salinity differences from 18 to 3 PSU.

Further evidence to support the case of EOF mode 2 being representative of gravitational circulation is provided by the timing of the reduced energy in the 14-day band of the wavelet spectrum of PC2 in relation to the salinity peaks at GIWW and Little Lake. The wavelet power at fortnightly timescales begins to decrease around Feb 2 and reaches a minimum around Mar 1, after which it begins to increase again (Figure 4.12). The Atchafalaya River, which discharges substantial amounts of freshwater into the Barataria estuary by way of the GIWW, shows a decline in discharge that begins in late Jan, and lasts through mid-Feb. Coincident increases in salinity occurred in both the GIWW and at the Little Lake site during this time, and salinity begins to drop again following the rise in Atchafalaya River discharge in late Feb (Figure 4.5). Kjerfve (1973) observed that tidal diffusion of Mississippi River plume water on the continental shelf into the estuary can also substantially decrease salinities in the system. Because Atchafalaya and Mississippi River discharges are highly correlated, these effects are difficult to separate quantitatively. Regardless of the source of freshwater, a decrease in estuarine salinities appears to have resulted in diminished baroclinic flows through the pass during this time period.

Though EOF mode 2 accounted for less than 10% of the observed current variability, its importance in the overall exchange through the pass can be seen by comparing the cumulative net transport at three locations in the water column. Approximately 300 km of water flowed seaward through the pass 1 m below the surface, while near the bottom 675 km of GOM water flowed into the Bay. Two-dimensional hydrodynamic models (e.g., Park 2002) are most reliable when vertical homogeneity can be assumed. That assumption is likely true throughout most of the shallow estuary, and

in the other three major passes (which are much shallower than Barataria Pass) where exchange with the GOM occurs. EOF mode 2 amplitudes were negative for the bottom seven current velocity bins. Taking the mean (0.93) and maximum (5.13) amplitudes for PC2 and multiplying them by the amplitudes of the bottom seven velocity bins for the second EOF eigenvector (Figure 4.8) gives mean and maximum inflow velocities of 3.7 and 21.3 cm s^{-1}, respectively, depth-averaged across the lower portion of the water column. Thus, salt flux into the estuary may be underestimated the two-dimensional hydrodynamic model.

Conclusions

Harmonic analysis indicated that tidally-forced flow accounted for nearly 85% of the total current variability in Barataria Pass. Under tropical tides, tidal excursions through the pass were sufficient to facilitate exchanges between Barataria Bay and the coastal ocean. On the other hand, during equatorial tides, tidal excursions were one-fifth the length of the pass and estuary-ocean exchange likely became largely dependent on processes that occur over longer timescales. Two modes of vertical structure in the subtidal flow field were identified. A barotropic mode, comprising over 90% of the subtidal current variability, was found to be forced primarily by cross-shelf winds. Alongshore winds were found to be relatively unimportant in forcing barotropic exchanges. The second mode, describing a vertically-sheared flow field where outflows near the surface were opposed by inflows near the bottom, accounted for roughly 8% of the current variability, and appeared to reflect gravitationally-driven estuarine circulation. Much of the energy in this mode existed over fortnightly timescales, apparently in response to fortnightly variations in tidal mixing energy brought about by the tropical-

equatorial cycle in the diurnal tidal currents. Wavelet analysis was effective in revealing a decrease in fortnightly variability in the second EOF mode occurring roughly midway through the study period. This was coincident with an apparent decrease in freshwater inflows to the system and a corresponding increase in estuarine salinity, and further suggested that the second EOF mode was indicative of baroclinic circulation.

Literature Cited

Angelovich, J.W. 1976. Environmental studies of the south Texas outer continental shelf, 1975. U.S. Department of Commerce, NOAA. Washington, D.C.

Banas, P.J. 1978. An investigation of the circulation dynamics of a Louisiana bar-built estuary. M.S. thesis. Louisiana State University, Baton Rouge, LA.

Bendat, J.S. and A.G. Piersol. 1993. Engineering Applications of Correlation and Spectral Analysis, Second Edition, Wiley, New York.

Byrne, P., M. Borengasser, G. Drew, R.A. Muller, B.L. Smith and C. Wax. 1976. Barataria Basin: Hydrologic and climatologic processes. Louisiana State University Center for Wetland Resources. Sea Grant Publ. No. LSU-T-76-010.

Chuang, W.S. and W.J. Wiseman, Jr. 1983. Coastal sea level response to frontal passages on the Louisiana-Texas shelf. Journal of Geophysical Research 88: 2615-2620.

de Miranda, L.B., B.M. de Castro, and B. Kjerfve. 1998. Circulation and mixing due to tidal forcing in the Bertioga Channel, Sao Paulo, Brazil. Estuaries 21: 204-214.

Elliott, A.J. and D.P. Wang. 1978. The effect of meteorological forcing on the Chesapeake Bay: the coupling between and estuarine system and its adjacent coastal waters. In: Hydrodynamics of Estuaries and Fjords (ed. J.C.J. Nihoul), Elsvier Scientific Pulb. Co., Amsterdam, pp 127-145.

Emery, W.J. and R.E. Thompson. 2001. Data Analysis Methods in Physical Oceanography. Elsevier, Amsterdam.

Garrett, C. and B. Toulany. 1982. Sea level variability due to meteorological forcing in the northwest gulf of St. Lawrence. Journal of Geophysical Research 87: 1968-78.

Griffin, D.A. and P.H. LeBolnd. 1990. Estuary-ocean exchange controlled by spring-neap tidal mixing. Estuarine, Coastal and Shelf Science 30: 275-305.

Grinsted, A., S. Jevrejeva, and J. Moore. 2004. Application of the cross wavelet transform and wavelet coherence to geophysical time series 11: 561-566.

Hansen, D.V. and M. Rattray. 1965. Gravitational circulation in straits and estuaries. Journal of Marine Research 23: 104-122.

Janzen, C.D. and K.C. Wong. 2002. Wind-forced dynamics at the estuary-shelf interface of a large coastal plain estuary. Journal of Geophysical Research 107 (C10), 3138, doi:10.1029/2001JC000959.

Kjerfve, B. 1973. Dynamics of the water surface in a bar-built estuary. Ph.D. dissertation. Louisiana State Uinversity, Baton Rouge, La.

Large, W.G. and S. Pond. 1981. Open ocean momentum flux measurements in moderate to strong winds. Journal of Physical Oceanography 11: 324-336.

Masson, D. and P.F. Cummins. 2000. Fornightly modulation of the estuarine circulation in Juan de Fuca Strait. Journal of Marine Research 58: 439-463.

Park, D. Hydrodynamics and freshwater diversion within Barataria Basin. Ph.D. dissertation. Louisiana State University. Baton Rouge, LA.

Peters, H. 1997. Observations of stratified turbulent mixing in an estuary: neap-to-spring variations during high river flow. Estuarine, Coastal and Shelf Science 45: 69-88.

Peters, H. 1999. Spatial and temporal variability of turbulent mixing in an estuary. Journal of Marine Research 57: 805-845.

Preisendorfer, R.W. 1988. Principal Component Analysis in Meteorology and Oceanography. Elsevier, Amsterdam. 425 pp.

Pritchard, D.W. 1955. Estuarine circulation patterns. Proceedings of the American Society of Civil Engineers 81, No. 717.

Shaw, R.F., W.J. Wiseman, Jr., R.E. Turner, L.J. Rouse, R.E. Condrey, and F.J. Kelly. 1985. Transport of larval Gulf menhaden *Brevoortia patronus* in continental shelf waters of western Louisiana: a hypothesis. Transactions of the American Fisheries Society 114: 452-460.

Simpson, J.H. and J.R. Hunter. 1974. Fronts in the Irish Sea. Nature 250: 404-406.

Swarzenski, C.M. 2002. Surface-water hydrology of the Gulf Intracoastal Waterway in south-central Louisiana 1996-99. U.S. Geological Survey Professional Paper 1672.

Torrence, C., and G.P. Compo. 1998. A practical guide to wavelet analysis, Bulletin of the American Meteorological Society 79: 61-78.

Torrence, C. and P. Webster. 1999. Interdecadal changes in the ENSO-monsoon system. Journal of Climate 12: 2679-2690.

Valle-Levinson, A. 1995. Observations of barotropic and baroclinic exchanges in the lower Chesapeake Bay. Continental Shelf Research 15: 1631-1647.

Wang, D.P. 1979. Subtidal sea level variations in the Chesapeake Bay and relations to atmospheric forcing. Journal of Physical oceanography 9: 413-421.

Wong, K.C. 1990. Sea level variability in Long Island Sound. Estuaries 13: 362-372.

Wong, K.C. 2002. On the wind-induced exchange between Indian River Bay, Delaware and the adjacent continental shelf. Continental Shelf Research 22: 1651-1668.

Wong, K.C and J.E. Moses-Hall. On the relative importance of the remote and local wind effects to the subtidal variability in a coastal plain estuary. Journal of Geophysical Research 89: 18393-18404.

CHAPTER V.

SUMMARY AND CONCLUSIONS

This study examined the interactions of wind, river, and tidal influences on water levels, sediment loading, and estuary-shelf exchange in the subestuaries of the Mississippi River delta. Wind influences have been studied extensively in open bay estuaries such as the Chesapeake , the Delaware , and Long Island Sound. These system all communicate freely with the coastal ocean and can be characterized as relatively deep (on the order of 10 m or more). Wind-driven subtidal sea level fluctuations inside such estuaries are induced by coastal sea level oscillations at the estuary mouth, as well as by the wind stress component along the axis of the estuary. The former generally causes estuarine sea-level fluctuations inside the estuary that are spatially uniform in amplitude, while the latter induces a sea level slope where surface waters are pushed in a downwind direction by stress at the air-water interface.

As with many major river deltas worldwide, the Mississippi River deltaic plain is unlike the aforementioned estuaries. Vegetated marshes, tidal flats, circuitous channels, and other features frictionally dissipate waves propagating through these shallow, productive systems. Thus, direct forcing by local wind stress over the estuary surface is apparently negligible, owing to the lack of significant fetch. Instead, atmospheric forcing occurs almost entirely through remote forcing, where alongshore winds facilitate estuary-shelf exchange through Ekman convergence at the coast. The highly-frictional nature of the deltaic landscape causes the estuary to act as a low-pass filter to remote atmospheric forcing, where high-frequency, coastally-induced fluctuations are significantly damped, and the damping increases with distance from the estuary mouth. This frequency-

dependent damping effectively eliminates tidal variability in the upper estuary. A frequency-dependent analytical model, previously used in other studies to describe sea level dynamics driven by coastal forcing in deeper, less frictional systems, was applied in the shallow Breton Sound estuary. In contrast to deeper systems where coastally-induced fluctuations exhibit little or no frictional attenuation inside the estuary, these fluctuations in the shallow, frictional Breton Sound estuary show strong frequency-dependent amplitude reductions that extend well into the subtidal frequency spectrum. Thus, Mississippi River floodplain estuaries, like Breton Sound, are particularly in important for storm surge protection, given their higher potential for frictional attenuation.

While the response to coastal forcing in the microtidal, deltaic Breton Sound estuary is clearly different from the response observed in drowned river valley estuaries, it is important to point out that the dampened response may not be ubiquitous to all deltas. Large tidal amplitudes in macrotidal deltas will have the overall effect of increasing the average depth h. Because frictional attenuation is proportional to the ratio between the frictional attenuation and natural frequencies (ω_f / ω_r), increasing h will have the overall effect of decreasing the numerator ($\omega_f = C_D / h$) and increasing the denominator ($\omega_r = \sqrt{gh} / L$); this results in a decrease in the ratio ω_f / ω_r and a proportional decrease in frictional attenuation.

A 30 to 45 cm maximum upper estuary water level response to discharge through the river diversion indicated by the transfer function suggests that, at least in the upper estuary, the river diversion has the capacity to induce high stages and subsequent sheet flow necessary to deliver fluvial materials to the marsh interior. Such a response was not

detected at the lower estuary site, suggesting that the diversion has a sea-level impact radius that lies somewhere between 7 and 30 km.

Fluvial sediment loading to the Mississippi River deltaic plain was estimated using a combination of hourly velocity measurements and turbidity measurements over a two-year period. Annual loading rates on the order of 1×10^5 metric tons yr^{-1} were observed, and approximately half of that occurred during two two-week pulsed 185 m^3 s^{-1} diversions each year. Sediment delivery during each pulse was highly variable (11300 to 43800 metric tons), and was greatest when pulses coincided with rising limbs of Mississippi River flood events. Overland flow, a necessary transport mechanism for sediments to reach the subsiding backmarsh regions, was induced only when diversion discharge exceeded 100 m^3 s^{-1}. This circumstance suggests that timing and magnitude of diversion events are both important factors governing marsh sediment deposition to coastal wetlands in the receiving basin of river diversions – timing is important to maximize sediment loading into the estuary, and the magnitude determines whether or not sheet flow and associated sediment delivery to the backmarsh regions occurs.

Using Wheelock's (2003) estimate of a 57 km^2 impact area and assuming a sediment density of 1.4 metric tons m^{-3} (Kesel 1989), an average annual deposition rate of 1.3 mm yr^{-1} is obtained. This estimate is based on the unlikely assumption that 100% of the introduced sediment is sequestered and deposited in the upper 6 km of the estuary; thus the rate mentioned above should be considered an upper bound. Nevertheless, it is insufficient to offset RSLR in the upper Breton Sound estuary, estimated to be 2.8 to 3.8 mm yr^{-1}. Maximizing diversion operations throughout an average river year could increase the annual deposition rate such that it exceeds RSLR. Yet even if such a plan

was implemented, RSLR would only be offset in the upper 6 km of the estuary. Thus, large diversions may need to be implemented at multiple sites along the river if RSLR is to be offset throughout the estuary through increased sedimentation.

While a sea-level response to the Caernarvon diversion was observed to extend between 7 and 30 km downestuary from the diversion structure, the depositional impact area of the diversion only extended about 6 km downestuary from the structure. Thus, the impact region of the diversion varies, depending the characteristic of interest. This point is important when considering the overall biogeochemical impact of diversions or any kind of periodic fluvial input to a deltaic estuary. For example, while diversion-induced flooding in the upper 6 km of the estuary may be beneficial by facilitating sedimentation, diversion-induced flooding of sediment-poor water 20 km downestuary may benefit wetland productivity through nutrient additions (Day et al. 2003)., or perhaps harm them by flood-stressing plant communities (McKee and Mendelssohn 1989).

To more closely examine marine influences on deltas forced by the remote atmospheric mechanism, estuary-shelf exchange between the Mississippi River delta and the Gulf of Mexico was observed with an ADCP located in Barataria Pass. Hourly measurements were made between Dec 2002 and Apr 2003. Tidal exchange accounted for greater than 80% of the total variance of flow in the pass, and was forced almost entirely by the K_1 and O_1 constituents. Tidal excursions were on the order of 30 km during tropical tides, but excursions were insufficient to effect complete exchange through the pass during equatorial tides. EOF analysis identified two dominant vertical structures in the subtidal exchange. Cross-wavelet analysis indicated that the barotropic mode of subtidal exchange, which accounted for over 90% of the subtidal flow variance,

was most coherent with north-south (cross-shelf) wind stress, while east-west (alongshore) wind stress played a secondary role. The second mode of subtidal exchange extracted from the EOF analysis displayed a vertical structure that was consistent with baroclinic estuarine circulation, and showed a pronounced fortnightly periodicity. The fortnightly oscillations varied 180º out of phase with the diurnal tidal current amplitude in the pass, suggesting that gravitational circulation in the pass was modulated by variations in tidal stirring power. A decrease in the wavelet power of the second EOF mode of circulation at fortnightly timescales coincided with a decrease in freshwater inputs to the estuary and an increase in estuarine salinities, suggesting that riverine forcing may have further modulated gravitational exchange through the pass over longer timescales.

It is interesting that the two adjacent regions of the Mississippi River deltaic plain studied here, the Breton Sound estuary and the Barataria estuary, showed a differential response to remote wind forcing. The response of the Breton Sound estuary was consistent with classical coastal Ekman dynamics, where winds blowing downcoast (in the sense of Kelvin wave propagation) resulted in an influx of water into the estuary. To the contrary, inflows through Barataria Pass into the Barataria estuary were forced most effectively through landward-wind stress blowing in a cross-shelf direction. This incongruity may result from geographical differences between the two subestuaries. While waters outside Breton Sound can respond coastal Ekman fluxes unhindered by geographical features, Ekman transport of coastal waters outside of Barataria Bay may be impeded by the presence of the Mississippi River and the birdfoot delta.

Another explanation may lie in the morphological differences between the two subestuaries. The mouth of Breton Sound has no tidal constrictions, and as such acts

very much like an open coastal embayment, showing a typical Ekman response to coastal winds. Exchange at the mouth of Barataria Bay, on the other hand, is constricted through a series of tidal passes at the bottom of the bay. Thus, through the local atmospheric forcing mechanism, cross-shelf winds tend to cause a setup across the bay. A northward wind may cause increased water levels the upper bay, and decreased levels in the lower bay. This dynamic produces a pressure gradient across the pass that favors the inflow of Gulf waters into the bay. The reverse may occur during southward winds: sea level sets up in the lower bay near the pass, causing sea levels inside the pass to exceed those immediately outside, and forcing a barotropic outflow through the constriction.

The presence of the baroclinic EOF mode has important implications for model studies between estuaries and continental shelves. For example, treating only the depth-integrated flow between these two regimes can be misleading. As shown in this study, the depth dependent flow structure contribute critically to exchange between the two regimes. Overlooking this mode of exchange could underestimate salt flux into the estuary. Hydrodynamic models are often the cornerstone for landscape change models that attempt to predict phenomena such as coastal land loss. Because this land loss is accelerated by saltwater intrusion, land loss projections obtained from such models may be artificially low.

Literature Cited

Day, J.W., J. Ko, J. Cable, J.N. Day, B. Fry, E. Hyfield, D. Justic, P. Kemp, R. Lane, H. Mashriqui, E. Reyes, S. Rick, G. Snedden, E. Swenson, P. Templet, R. Twilley, K. Wheelock and B. Wissel. 2003. PULSES: The importance of pulsed physical events for Louisiana coastal floodplains and watershed management, pp. 693-699. First Interagency Conference on Research in the Watersheds, October 27-30, 2003. U.S. Department of Agriculture, Agricultural Research Service, Benson, Arizona.

Kesel, R.H. 1989. The roll of the Mississippi River in wetland loss in southeastern Louisiana, U.S.A. Environmental Geology and Water Science 13: 183-193.

McKee, K.L. and I.A. Mendelssohn. 1989. Response of a freshwater marsh plant community to increased salinity and increased water level. Aquatic Botany 34: 301-316.

Wheelock, K.W., 2003. Pulsed river flooding effects on sediment deposition in Breton Sound Estuary, Louisiana. M.S. Thesis. Louisiana State Univ., Baton Rouge, LA.

VITA

Gregg Alan Snedden was born on May 4, 1971, in Des Moines, Iowa. He is the son of Al and Camille Snedden and the younger brother of Suzette Gourley. He attended Normal Community High School, in Normal, Illinois, and graduated in 1989. Gregg attended the University of Illinois at Urbana-Champaign and studied aquatic ecology, receiving a degree of Bachelor of Science in Ecology, Ethology, and Evolution in May 1993.

Gregg entered the graduate program in the School of Forestry, Wildlife, and Fisheries at Louisiana State University in August 1993. His thesis involved using radiotelemetry to study floodplain movements of spotted gar in the Atchafalaya River Basin. He was awarded a Master of Science degree in fisheries in May 1997. In August 1997, after briefly working for the Florida Game and Freshwater Fish commission, Gregg returned to Louisiana and began working as a wetland ecologist for the Louisiana Department of Natural Resources, where he monitored ecosystem restoration in the Mississippi River delta associated with Mississippi River diversion projects.

In August 2000, Gregg began working as a research associate at Louisiana State University's Coastal Ecology Institute. He concurrently enrolled as a doctoral student in the Department of Oceanography and Coastal Sciences at Louisiana State University. He will earn a doctoral degree in oceanography and coastal sciences in May 2006. Gregg now works as a post-doctoral research fellow for the Center for Marine Science at the University of North Carolina at Wilmington.